Phase transitions in sampling and error correction in local Brownian circuits

Subhayan Sahu [1,*] and Shao-Kai Jian [2,†]

[1]*Perimeter Institute for Theoretical Physics, Waterloo, Ontario, Canada N2L 2Y5*
[2]*Department of Physics and Engineering Physics, Tulane University, New Orleans, Louisiana 70118, USA*

We study the emergence of anticoncentration and approximate unitary design behavior in local Brownian circuits. The dynamics of circuit-averaged moments of the probability distribution and entropies of the output state can be represented as imaginary-time evolution with an effective local Hamiltonian in the replica space. This facilitates large-scale numerical simulation of the dynamics in $1 + 1$ dimensions of such circuit-averaged quantities using tensor network tools as well as identifying the various regimes of the Brownian circuit as distinct thermodynamic phases. In particular, we identify the emergence of anticoncentration as a sharp transition in the collision probability at $\ln N$ timescale, where N is the number of qubits. We also show evidence for a specific classical approximation algorithm undergoing a computational hardness transition at the same timescale. In the presence of noise, we show there is a noise-induced first-order phase transition in the linear cross entropy benchmark when the noise rate is scaled down as $1/N$. At longer times, the Brownian circuits approximate a unitary 2-design in $O(N)$ time. We directly probe the feasibility of quantum error correction by such circuits and identify a first-order transition at $O(N)$ timescales. The scaling behaviors for all these phase transitions are obtained from the large-scale numerics and corroborated by analyzing the spectrum of the effective replica Hamiltonian.

I. INTRODUCTION

Random quantum circuits (RQCs) play a pivotal role in both quantum dynamics theory and quantum information theory, offering insights into fundamental aspects such as quantum chaos, out-of-time correlation functions, and entanglement entropy [1–5]. Closely related to RQCs, the random tensor network serves as a valuable tool for investigating the anti–de Sitter/conformal field theory correspondence, a theory aimed at understanding quantum gravity through quantum entanglement [6]. Additionally, random quantum circuits find extensive applications in quantum information theory, including quantum advantage [7–10], quantum error correction [11–13], etc.

Random circuits are expected to be a toy model capturing the following properties of generic quantum circuits: They output states of high complexity and generate maximal entanglement between initially disconnected regions. An important question is characterizing the time (depth) required for achieving the high complexity. How do we characterize the complexity of random circuits? In this work we focus on two distinct features: anticoncentration and unitary design.

Consider a circuit C acting on an initial simple state (the product state of $|0\rangle$ on all qubits) with the output state being measured in the computational basis to obtain a distribution over measurement outcomes $p_C(s) = |\langle s|C|0\rangle|^2$.

Anticoncentration is the property that $p_C(s)$ is well spread over all bit strings s. Certifying that the circuit is anticoncentrated is crucial in guaranteeing that the RQC simulation is classically hard and is a promising route towards demonstrating quantum advantage [7,9,10,14,15].

At long enough depths, the RQC has a stronger notion of complexity: It becomes an approximate unitary design. A unitary ensemble is said to be a k-design if it approximates a global Haar random unitary in its first k moments. In particular, ensuring that a RQC has achieved the 2-design property is enough for the RQC to be maximally decoupling. Consider a system A, initially maximally entangled with a reference R, that is subjected to a circuit C, before being coupled to an environment E. The initial encoding via C is said to have the decoupling property if the joint density matrix on $R \cup E$ is approximately factorizable $\rho_{RE} \approx \rho_R \otimes \rho_E$. This can also be associated with the RQC dynamically generating a quantum error correcting code [11–13].

Several avenues of research on RQCs have established that anticoncentration and unitary design occur at parametrically distinct timescales. Suppose we consider circuits with spatial local connectivity in d dimensions. Past research has shown that ensembles of RQCs with Haar random local gates achieve anticoncentration and the unitary design in $O(\ln N)$ [16] and $O(N^{1/d})$ [17–19] timescales, respectively, where N denotes the number of qubits. Note that both anticoncentration and the 2-design property are diagnosed by nonlinear properties of the quantum state generated by the circuits. This makes numerically simulating these properties for local Haar random circuits hard and limited to modest system sizes and short times. Hence, much of the research on RQCs has depended

---

*ssahu@perimeterinstitute.ca
†sjian@tulane.edu

on proving analytical bounds, classically simulable Clifford circuits, and perturbations around semiclassical limits, such as large local Hilbert space dimensions.

In this work we provide a minimal model which allows us to do an efficient and guaranteed numerical simulation of the quantum informational quantities probing anticoncentration and the 2-design property of large random circuits using tensor network technology. We take the approach of directly representing the informational quantities averaged over the circuit ensemble as a linear observable in a replicated Hilbert space. Here replicas are simply exact copies of the original system and the informational observables probe the correlation between different replicas. We study a particular ensemble of RQCs, namely, local Brownian circuits [20–24].

These Brownian qubit models can be defined on any graph where each vertex hosts a qubit, with nearest-neighbor Brownian interaction generating the unitary evolution. Remarkably, the real-time evolution of circuit-averaged nonlinear observables of the density matrix can now be realized as imaginary-time evolution in the replica space. The Hilbert space for k replicas is simply the combination of a forward contour and a backward contour for real-time evolution for each replica; so the local Hilbert space encompasses $2k$ spins. After averaging of Brownian couplings, the quantum dynamics reduces to a Hermitian replica qubit Hamiltonian with the same locality properties as the initial interaction graph. This model not only establishes a clear mapping between various quantum information quantities and those of a quantum spin model, but also transforms the problem of quantum dynamics into a thermodynamic problem.

Furthermore, imaginary-time evolution with local Hamiltonians is guaranteed to be efficient in one dimension using simple matrix product state and time-evolving block decimation (TEBD) algorithms [25–27]. This allows us to perform large-scale simulations of these informational quantities in a $(1+1)$-dimensional circuit. As an example, we can simulate the averaged Rényi-2 entanglement properties of a Brownian circuit on $N \sim O(100)$ qubits for $t \sim O(N)$ depths in a few minutes on a standard laptop.

The effective Hamiltonian approach also provides a statistical mechanical description of different regimes of RQCs as distinct phases, separated by phase transitions. These phases can be described within a generalized Landau framework involving multiple replicas, where the relevant symmetry is the replica permutation symmetry [28] (when we introduce multiple identical copies of the system, they can be permuted among each other without changing the effective description). Specifically, in the two-replica scenario that we focus on in this work, the effective Hamiltonian has a $\mathbb{Z}_2$ symmetry corresponding to a relative swap between the two real-time contours, which turns out to be the relevant symmetry for nonlinear observables of the density matrix. This effective Hamiltonian is essentially a $\mathbb{Z}_2$ Ising model in the replica space, and the phases of quantum information and their phase transitions are associated with the various phases and critical properties of this Ising model.

Using large-scale numerics of the Brownian circuit model, we can directly probe the dynamical properties of the quantum informational quantities and identify the saturation to anticoncentration (at approximately $\ln N$ depth) and the

2-design property (at approximately N depth) of the RQC as sharp transitions, confirmed by careful finite-size scaling of the numerical data. This can be understood analytically by investigating the spectral properties of the effective Hamiltonian. The anticoncentration transition can also be directly associated with a transition in the computational hardness of classically simulating the output distribution. To show this, we provide evidence that a specific algorithm for simulating the output distribution [29] undergoes a hardness transition at approximately $\ln N$ depth.

In order to study the 2-design transition, we focus on investigating the feasibility of the Brownian circuit as a quantum error correcting code, by directly simulating a quantity akin to the mutual information between the reference and environment in the decoupling setup, named mutual purity [30]. The mutual purity is a two-replica quantity and has recently been shown to provide a bound for the error correction capabilities of RQCs in [30]. We show that the mutual purity undergoes a first-order transition in $O(N)$ time, after which the Brownian circuit approximates the global Haar random unitary for coding purposes. This coding transition is a first-order pinning transition, driven by boundary conditions determining the mutual purity, akin to [13]. Furthermore, the mutual purity contributes to a bound for the failure probability for correcting errors after the encoding by the RQC. By numerically computing the mutual purity for different error models after the 2-design transition, we can also find a first-order threshold transition for the code distance.

As mentioned earlier, sampling of RQC outcome states is one of the most promising routes towards demonstration of quantum advantage in near-term quantum devices [7,9,10,14,15]. However, real quantum devices suffer from noise. In order to benchmark the noisy quantum device, an estimate of the fidelity of the output state is desirable. One proposal for an efficient estimate for the fidelity is the linear cross-entropy benchmark χ_{XEB}, and a high score in this benchmark suggests that the RQC simulation is classically hard [14]. However, it has recently been understood that with local noise models, there is a noise-induced phase transition (NIPT) in the linear cross-entropy benchmarking [8,31–33]. In the weak-noise regime, χ_{XEB} provides a reliable estimate of fidelity, and in the strong-noise regime, it fails to accurately reflect fidelity. Furthermore, this implies that in the strong-noise regime, classical simulation can yield a high score in the cross-entropy benchmark [34,35], without necessarily solving the sampling task. The noise model can be incorporated in our Brownian circuit setup, where the noise serves as an explicit replica-permutation symmetry-breaking field [36]. Using a combination of numerical and analytical tools, we characterize the NIPT in benchmarking by identifying it as a first-order phase transition in the effective Hamiltonian picture.

We first briefly summarize the results of the paper. The main results of the paper are represented in Fig. 1 and Table I.

Anticoncentration. We probe anticoncentration in the $(1+1)$-dimensional Brownian circuit U by computing the collision probability [16]. Consider the setup where a RQC of a certain depth acts on the $|0^{\otimes N}\rangle$ state of N qubits, following which all the qubits are measured in the computational basis, resulting in a bit string $x \in \{0, 1\}^N$. The collision probability is defined as the circuit-averaged probability that two independent
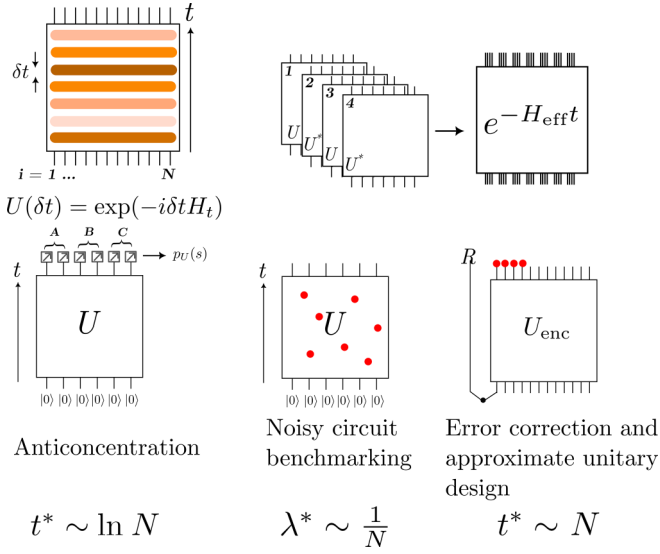
FIG. 1. We consider local Brownian circuits acting on qubits in a chain. Averaging the replica dynamics $U \otimes U^* \otimes U \otimes U^*$ leads to an imaginary-time evolution with a local Hamiltonian in replica space, H_{eff}. We can simulate this imaginary-time evolution in $1 + 1$ dimensions efficiently with tensor networks. We study three scenarios, i.e., anticoncentration, noisy circuit benchmarking, and approximate unitary design (and consequently error correction), and find distinct quantum informational phases in different time and noise regimes, separated by phase transitions. These results are corroborated using large-scale numerics and analyzing the spectrum of H_{eff}.

measurement outcomes with the same circuit realization produce the same result, defined as $Z = \mathbb{E} \sum_x |\langle x|U|0^{\otimes N}\rangle|^4$, where the averaging of approximately $\mathbb{E}$ is done over all realizations of the circuit.

In the context of the effective Ising Hamiltonian H_{eff} description, we demonstrate that Z equates to the transition probability between an imaginary-time-evolved state from the initial state and a quantum paramagnetic state (defined in a later section). The imaginary-time evolution gradually projects the initial state onto the ground state of H_{eff}, which corresponds to $Z \sim 2^{-N}$. However, in finite time t, excited-state contributions result in $2^N Z = 2 + S_\Delta e^{-\Delta t}$, where Δ (S_Δ) denotes the energy gap (entropy) of the excitation.[1] The anticoncentration transition thus occurs at $t = \frac{1}{\Delta} \ln S_\Delta \sim \ln N$, representing a depth-induced computational transition. The $\ln N$ results arise from the nature of the elementary excited states of the Ising model and can be confirmed by direct large-scale simulation of the imaginary-time evolution.

Computational hardness transition. We probe the computational hardness of sampling from the probability distribution in the measurement outcome in the earlier setup, i.e., $p_U(x) = |\langle x|U|0^{\otimes N}\rangle|^2$. By studying the Rényi-2 version of conditional mutual information (CMI) of $p_U(x)$ using numerics of the imaginary-time evolution, we probe the hardness of a specific

---

[1]In a one-dimensional chain with local couplings, the elementary excitation manifests as a domain wall, with a finite gap independent of the system size and an entropy proportional to the system size.

TABLE I. Transition point, nature of the transition, and asymptotic scaling for various information quantities for the Brownian circuit.

Anticoncentration and computational hardness
Depth-driven first order transition between different low energy eigenstates

		$t < t^* \sim \log N$	$t > t^*$
Collision probability $\sum_s p_U(s)^2$		$O(e^{N^c} 2^{-N})$	$O(2^{-N})$
Conditional mutual information $I^{(2)}(A : C | B)_{p_U}$		$O(e^{-N})$	$O(1)$

Noisy circuit benchmarking
Noise induced first order transition due to bulk symmetry breaking fields.

		$\lambda < \lambda^* \sim 1/N$	$\lambda > \lambda^*$
Linear XEB $2^N \sum_s p(s)q(s) - 1$		$e^{-N\lambda t}$	$e^{-\Delta t}$
Fidelity $\text{Tr}\mathcal{N}(\rho)\rho$		$e^{-N\lambda t}$ ($\lambda t \lesssim 1$)	$e^{-N\lambda t}$ ($\lambda t \lesssim 1$)

Error correction and approximate unitary design
Depth-induced first order domain wall depinning transition

		$t < t^* \sim N$	$t > t^*$
Mutual Purity		$O(2^{-N})e^{-t}$	$O(2^{-N})$

classical algorithm (patching algorithm) for approximately simulating the output distribution as introduced in [29]. We find that the Rényi-2 CMI undergoes a phase transition at $O(\ln N)$ time, with the same scaling behavior as the collision probability, signaling a computational hardness phase transition at the same depth. It must be noted that the theorem concerning the feasibility of the patching algorithm depends on the actual CMI and not necessarily its annealed Rényi-2 version that we study here. Hence, our results provide evidence for a (classical) computational hardness transition and not a rigorous proof for it.

Phase transition in cross-entropy benchmarking of noisy Brownian circuits. Here we consider the following setup of two copies of the Brownian circuit: one that is affected by noise (denoted by the noisy channel $\mathcal{N}$) and another that undergoes the noise-free Brownian circuit. We can now update the effective Hamiltonian with explicit noise in one of the replicas, $H_{\text{eff}} \to H'_{\text{eff}}$. We can compute the fidelity $F = \text{Tr}[\mathcal{N}(\rho)\rho]$ of the noisy simulation by doing imaginary-time evolution with H'_{eff} (with local noise models, H'_{eff} remains local). We also compute the linear cross-entropy benchmark, defined as $\chi_{\text{XEB}} = 2^N \sum_x p(x)q(x) - 1$, where $p(x)$ and $q(x)$ represent the output distribution in the noise-free and noisy cases, respectively [14].

In H'_{eff}, noise explicitly breaks the Ising symmetry and subsequently pins the Ising spins. Consider a local (unital) noise model, with λ strength for each qubit (to be explicitly defined

later). Noise generically undermines the ferromagnetic phase that leads to anticoncentration and leads to erosion of the quantum advantage. This holds true for constant rate noise $\lambda \sim O(1)$. Through the mapping to the quantum Ising model, we discover that noise behaves as a relevant perturbation with a scaling dimension of 1. Therefore, when the noise rate scales inversely with respect to the size of the chain $\lambda \sim 1/N$, we get a noise-induced computational transition at some critical $\lambda^* \sim O(1/N)$. This transition essentially resembles a field-induced first-order transition and conforms to finite-size scaling with $\nu = \frac{1}{2}$, which we confirm numerically. Moreover, if the rate scales less (greater) than $1/N$, the noise is deemed irrelevant (relevant). This result is consistent with recent results on noise-induced phase transitions in cross-entropy benchmarking [8,31,32].

We also study whether this transition signals a transition in the computational hardness in the simulation of noisy Brownian circuits. By studying the Rényi-2 CMI of $p_{\mathcal{N}(U)}(x)$, we find that it does not undergo a hardness transition with depth for large enough depths and actually exponentially decays with time. This suggests that the $(1 + 1)$-dimensional noisy random circuits are efficiently simulable in the long-time limit, even in the presence of infinitesimal-scale noise.

Coding transitions. We encode some local information (a reference qubit R) in the entire system A using the Brownian circuit and probe the effectiveness of this encoding as a quantum error correcting code. After encoding, the state on A is affected by noise, which can be identified as a unitary coupling with the environment E. Mutual purity $\mathcal{F}_{RE}$ [30] is a two-replica quantity which upper bounds the trace distance between the initial encoded state and the error-affected encoded state after error correction using a recovery channel [37,38].

From the effective Hamiltonian perspective, the mutual purity can be represented as a transition probability between two ferromagnetic states. In particular, we find that at short times the mutual purity decays exponentially, which can be identified with domain-wall configurations pinned between the initial and final states, while after $t \sim O(N)$ time the domain walls get depinned, resulting in the saturation of the mutual purity to a global Haar value, i.e., realizes an approximate 2-design. Using large-scale numerics, we are able to directly probe this transition to a 2-design as a first-order depinning transition. Furthermore, since the mutual purity determines the feasibility of error correction after the application of noise, we find a first-order threshold transition in the fraction of qubits which are affected by noise. The critical fraction can be identified as a lower bound for the code distance of the Brownian circuit as a quantum error correcting code.

The paper is organized as follows. Section II presents an introduction to the Brownian circuit model and a derivation of the effective Hamiltonian for $k = 2$ replicas. In Sec. II B we describe the symmetries of the effective Hamiltonian and provide a heuristic description of the phase diagrams. In Sec. III we discuss the anticoncentration and computational hardness transition. In Sec. IV we investigate the noise-induced phase transition in benchmarking noisy Brownian circuits. In Sec. V we study the error correcting properties of the Brownian circuit and probe the transition to an approximate 2-design.

We conclude by discussing the implications of this work and future directions in Sec. VI.

II. LOCAL BROWNIAN CIRCUITS

We consider a Brownian circuit on N qubits in a chain, with the Hamiltonian

$$H_t = \sum_{\langle i,j \rangle}^{N} \sum_{\alpha,\beta} J_{t,ij}^{\alpha\beta} \sigma_i^\alpha \sigma_j^\beta, \tag{1}$$

where α and β label the Pauli indices of the local Pauli matrices σ_i, interacting between nearest-neighbor pairs $\langle i, j \rangle$. In addition, $J_{t,\alpha\beta}$ is a normal random variable uncorrelated in time, defined via the properties

$$\mathbb{E}[J_{t,ij}^{\alpha\beta}] = 0,$$

$$\mathbb{E}[J_{t,ij}^{\alpha\beta} J_{t',ij}^{\alpha'\beta'}] = \frac{J\delta_{tt'}}{\delta t} \delta_{\alpha\alpha'} \delta_{\beta\beta'}, \tag{2}$$

where $\mathbb{E}$ denotes the average according to the distribution.

A. Effective Hamiltonian description

We integrate over the random couplings to get an effective Hamiltonian in the replica space. To this end, let us first consider a unitary evolution of a density matrix, $\rho' = U\rho U^\dagger$. Explicitly writing out the indices, it is

$$\rho'_{a'b'} = \sum_{a,b} U_{a'a} \rho_{ab} U_{bb'}^\dagger = \sum_{a,b} U_{a'a} U_{b'b}^* \rho_{ab}. \tag{3}$$

In the second term, we transpose $U^\dagger$ and use the fact that $(U^\dagger)^T = U^*$. Viewed as a tensor, the time evolution can be expressed by an operator $U \otimes U^*$ acting on a state $\sum_{ab} \rho_{ab}|a\rangle \otimes |b\rangle$. This is essentially the Choi-Jamiołkowski isomorphism (the operator-state mapping) [39,40]. Now we can extend this to two replicas. Since most of our discussion focuses on two replicas, we derive an effective Hamiltonian for two replicas. Note that it is straightforward to generalize the derivation to k replicas and to an arbitrary number of qubits on each node [24]. Because the random couplings at different time are uncorrelated, the central quantity is the instantaneous time evolution (for a small time interval δt) operator for the four contours,

$$U_1(\delta t) \otimes U_2(\delta t)^* \otimes U_3(\delta t) \otimes U_4(\delta t)^*, \tag{4}$$

where U_a, $a = 1, 2, 3, 4$, denotes the unitary evolution operator generated by the Brownian spin Hamiltonian $U_a(\delta t) = e^{-i\delta t H_{t,a}}$ acting on the four Hilbert spaces. It includes two replicas, each of which contains a forward contour $a = 1, 3$ and a backward contour $a = 2, 4$. The complex conjugate is due to the Choi-Jamiołkowski isomorphism, as demonstrated above.

The average over the random coupling reads

$$\mathbb{E}[U_1(\delta t) \otimes U_2(\delta t)^* \otimes U_3(\delta t) \otimes U_4(\delta t)^*]$$

$$= \int DJ P[J] \exp\left(\sum_a (-i)^a \delta t \sum_{\langle i,j \rangle} \sum_{\alpha,\beta} J_{t,ij}^{\alpha\beta} \tau_{i,a}^\alpha \tau_{j,a}^\beta\right), \tag{5}$$

where $\tau_{i,1}^\alpha = \tau_{i,3}^\alpha = \sigma_i^\alpha$ and $\tau_{i,2}^\alpha = \tau_{i,4}^\alpha = (\sigma_i^\alpha)^*$, $\alpha = 1, 2, 3$. The sign factor $(-i)^a$ appears due to the conjugated unitary on each replica. Here σ^α denotes the Pauli matrix, and the complex conjugate for the $a = 2, 4$ contour is due to the backward evolution. In addition, $DJ = \prod_{\langle i,j \rangle} \prod_{\alpha,\beta} dJ_{t,ij}^{\alpha\beta}$ and $P[J]$ denotes the Gaussian distribution specified by (2). Integrating over the random couplings results in an effective Hamiltonian

$$\mathbb{E}[U_1(\delta t) \otimes U_2(\delta t)^* \otimes U_3(\delta t) \otimes U_4(\delta t)^*] = e^{-\delta t H_{\text{eff}}}, \quad (6)$$

with

$$H_{\text{eff}} = \frac{J}{2} \sum_{\langle i,j \rangle} \sum_{a,b} (-1)^{a+b} (\vec{\tau}_{i,a} \cdot \vec{\tau}_{i,b})(\vec{\tau}_{j,a} \cdot \vec{\tau}_{j,b}). \quad (7)$$

This Hamiltonian describes a spin chain with four spins per site, denoted by $\vec{\tau}_{i,a}$, $a = 1, 2, 3, 4$. In the following we will see that this Hamiltonian can describe various information phases and phase transitions, such as a dynamical computational transition and error correcting transition. Similarly, for a finite-time evolution, we have

$$\mathbb{U} \equiv \mathbb{E}[U_t \otimes U_t^* \otimes U_t \otimes U_t^*] = e^{-H_{\text{eff}} t}. \quad (8)$$

Here we use $U_t = \exp(-i \int dt H_t)$ to denote the unitary generated by the Brownian circuit for a time interval t.

Numerical implementation

We simulate imaginary-time evolution in the replica Hilbert space using the TEBD algorithm. The local Hilbert space is $\mathbb{C}_2^{\otimes 4}$, reflecting the two replicas and two time contours per replica. To simulate $\exp(-t H_{\text{eff}})$ we now need to Trotterize the TEBD evolution with Δt as the time step; we take the energy scale $J = 1/\Delta t$. This ensures that $\Delta t H_{\text{eff}}$ is dimensionless with the energy scale set to 1 and with the evolved time t as non-negative integers. All calculations are performed using the TENPY library [41].

B. Replica permutation symmetry

The Hamiltonian (7) is invariant under replica relabeling and has the symmetry group

$$(S_2 \times S_2) \rtimes \mathbb{Z}_2, \quad (9)$$

where $S_2 \times S_2$ is the permutation group on the two-replica labels. The outer $\mathbb{Z}_2$ arises from the symmetry of shuffling between the two time-conjugated copies after taking the complex conjugation.[2] Put simply, each of the S_2 transformation swaps $\tau_{i,1}^\alpha \leftrightarrow \tau_{i,3}^\alpha$ or $\tau_{i,2}^\alpha \leftrightarrow \tau_{i,4}^\alpha$, whereas the $\mathbb{Z}_2$ exchanges $\tau_{i,1}^\alpha \leftrightarrow \tau_{i,2}^\alpha$ and $\tau_{i,3}^\alpha \leftrightarrow \tau_{i,4}^\alpha$ simultaneously.

It is easy to see that the Hamiltonian can be brought into a sum of squares

$$H_{\text{eff}} = \frac{J}{2} \sum_{\langle i,j \rangle} \sum_{\alpha,\beta} \left(\sum_a (-1)^a \tau_{i,a}^\alpha \tau_{j,a}^\beta \right)^2. \quad (10)$$

---

[2]Note that since the variance of coupling is independent of $\alpha = x, y, z$, the resultant Hamiltonian also enjoys a SU(2) symmetry for each site; however, our results do not rely on this symmetry.

Therefore, the eigenvalues are no less than zero. Two ground states are $|\text{id}\rangle\!\rangle^{\otimes N}$ and $|\text{swap}\rangle\!\rangle^{\otimes N}$, where

$$|\text{id}\rangle\!\rangle = \tfrac{1}{2}(|0000\rangle + |0011\rangle + |1100\rangle + |1111\rangle),$$

$$|\text{swap}\rangle\!\rangle = \tfrac{1}{2}(|0000\rangle + |1001\rangle + |0110\rangle + |1111\rangle). \quad (11)$$

Here we use $|0\rangle$ and $|1\rangle$ to denote $\pm$ eigenstates of the σ_z Pauli operator. The name of the state indicates that $|\text{id}\rangle\!\rangle$ is a product of an Einstein-Podolsky-Rosen (EPR) state of the first and second spins and an EPR state of the third and fourth spins, and $|\text{swap}\rangle\!\rangle$ is a product of an EPR state of the first and fourth spins and an EPR state of the second and third spins. Using the properties of EPR pairs, namely, $\tau_1 |\text{id}\rangle\!\rangle = \tau_2 |\text{id}\rangle\!\rangle$, $\tau_3 |\text{id}\rangle\!\rangle = \tau_4 |\text{id}\rangle\!\rangle$, $\tau_1 |\text{swap}\rangle\!\rangle = \tau_4 |\text{swap}\rangle\!\rangle$, and $\tau_2 |\text{swap}\rangle\!\rangle = \tau_3 |\text{swap}\rangle\!\rangle$, we can see that every square in the Hamiltonian vanishes, so these two states are ground states with zero energy.

The permutation symmetry is spontaneously broken by the ground state, and when the low-energy physics is concerned, our model is essentially equivalent to an Ising model. Note that we can organize the permutation transformation such that one of them permutes the second and fourth spins (we denote this by $S_2^r : \tau_{i,2}^\alpha \leftrightarrow \tau_{i,4}^\alpha$), while the other permutes both the first and third spins as well as the second and fourth spins. Then S_2^r can transform one ground state to the other and only S_2^r is spontaneously broken.

Our model (6) transforms the real-time evolution along the four contours into an imaginary-time evolution that progressively projects onto the ground-state subspace of the Hamiltonian described in Eq. (7). This imaginary-time evolution allows us to capture the dynamics of several important quantum information quantities. One such quantity is the collision probability, which measures the degree of anticoncentration and corresponds in the replica model to the overlap between the time-evolved state and a final state (to be specified later). The magnitude of this overlap is determined by the excitation gap present in the Hamiltonian (7). In one-dimensional systems, the elementary excitation takes the form of domain walls, which possess a finite-energy gap and exhibit logarithmic entropy. As a result, the process of anticoncentration requires a timescale proportional to $\ln N$, where N represents the system size.

C. Effective Hamiltonian with local noise

Since we would also like to investigate the effect of quantum noise, we now consider imperfect time evolution due to the presence of quantum errors. The unitary-time-evolution operators are replaced by a quantum channel. A local depolarization channel is given by

$$\rho \rightarrow (1 - \lambda)\rho + \frac{\lambda}{3} \sum_{\alpha=1,2,3} \sigma_i^\alpha \rho \sigma_i^\alpha, \quad (12)$$

where $0 \leqslant \lambda < \frac{3}{4}$ for complete positivity. Using the operator-state mapping, this can be mapped to

$$\mathcal{N}_i^{\text{depol}}(\lambda) = (1 - \lambda)I^{\otimes 2} + \frac{\lambda}{3} \sum_{\alpha=1,2,3} \sigma_i^\alpha \otimes (\sigma_i^\alpha)^*, \quad (13)$$

where I denotes the identity operator.

The noise can induce a transition of random circuit sampling [8,31]. An observable of such a transition is the

cross-entropy benchmarking (XEB), which we will describe in detail later. For now, let us just mention that XEB contains two distributions: one from a noiseless quantum circuit and the other from a noisy quantum circuit. Therefore, we are again concerned with only two replicas. Without loss of generality, we assume the noisy replica is described by the first two contours $a = 1, 2$ and the noiseless replica is described by the last two contours $a = 3, 4$. We upgrade the quantum channel to

$$\mathcal{N}_i^{\text{depol}}(\lambda) \rightarrow \mathcal{N}_i^{\text{depol}}(\lambda) \otimes I \otimes I. \tag{14}$$

The identity operators for the last two Hilbert spaces is clear since the second replica is noiseless. Thus, the noise occurs for the first replica with the first and second copies of the Hilbert space.

It is not hard to see that the channel can be equivalently described by a perturbation described by the effective Hamiltonian

$$H_{\text{depol}}(\lambda) = \frac{3}{4\delta t} \ln\left(\frac{1}{1 - \frac{4}{3}\lambda}\right) \sum_i \left(1 - \frac{1}{3}\sum_\alpha \tau_{i,1}^\alpha \tau_{i,2}^\alpha\right). \tag{15}$$

Here we assume the noise occurs at each site with the same strength. Since $0 \leqslant \lambda < \frac{3}{4}$ for the depolarizing channel, the prefactor is positive.

Essentially, the perturbation explicitly breaks the permutation symmetry. The state $|\text{id}\rangle\rangle^{\otimes N}$ is still an eigenstate of these two perturbations with eigenvalue zero, whereas the state $|\text{swap}\rangle\rangle^{\otimes N}$ obtains a finite positive energy, i.e.,

$$\langle\langle\text{swap}|^{\otimes N} H_{\text{depol}}(\lambda)|\text{swap}\rangle\rangle^{\otimes N} = \frac{3N}{4\delta t} \ln\left(\frac{1}{1 - \frac{4}{3}\lambda}\right). \tag{16}$$

Therefore, the presence of noise effectively lifts the degeneracy between the two ground states and biases the system towards the state $|\text{id}\rangle\rangle^{\otimes N}$. In the regime of low-energy physics, the noise can be treated as an external field that explicitly breaks the Ising symmetry and favors a particular state. For notation simplicity, we denote the local Zeeman energy by ϵ. For the depolarization channel, the effective Zeeman energy is $\epsilon = \frac{3}{4\delta t} \ln(\frac{1}{1 - \frac{4}{3}\lambda})$. When λ is small, we can deduce that $\epsilon \approx \frac{\lambda}{\delta t}$. Note that λ is dimensionless and δt is the unit of energy.

In the symmetry-breaking phase, the external field acts as a relevant perturbation with a scaling dimension of 1. Consequently, a first-order transition occurs at an infinitesimally small noise strength, which is independent of the system size. However, if the noise strength is appropriately scaled down by a factor of $1/N$, which compensates for its relevant scaling dimension, the transition can take place at a finite size-dependent noise strength given by $\epsilon \sim 1/N$. This noise-induced transition also manifests as a first-order phase transition. The first-order transition exhibits a finite-size scaling and is distinguished from a second-order transition [42]. We will confirm it via a systematic finite-size scaling.

III. ANTICONCENTRATION AND COMPUTATIONAL HARDNESS OF SAMPLING BROWNIAN CIRCUITS

A. Anticoncentration

It is well known that random circuits generate output states that are anticoncentrated, which roughly means that the probability distribution of the classical bit strings generated by measuring the output state of a random circuit in the computational basis is well spread out and not concentrated on a few bit strings. Naturally, this also implies that classical sampling of these bit strings will be hard. Two key ingredients underpin random circuit sampling. First, anticoncentration asserts that the distribution deviates only slightly from a uniform distribution. This property is typically required in hardness proofs. However, anticoncentration can be easily attained by applying a Hadamard gate to all qubits. Therefore, we need the second ingredient, randomness, to eradicate any discernible structure in the circuit. Given that randomness is inherent in our model, we are intrigued by whether the distribution exhibits anticoncentration and, if so, at what time (depth) it occurs. This indicates a transition in computational complexity, wherein the system shifts from a region that is easily achievable by classical means to a region that becomes challenging for classical algorithms.

When the random circuits are generated by a particular ensemble of local quantum gates, a key diagnostic of the complexity of the ensemble is the time it takes to anticoncentrate the output states. Concretely, we can compute the collision probability, which is defined as the probability that the measurement outcomes of two independent copies of the random circuit agree with each other, i.e., $\sum_s p_U(s)^2$, where $p_U(s) = |\langle s|U|0\rangle|^2$, for a given bit string s. We are interested in the ensemble-averaged collision probability which can be readily expressed as the transition amplitude in the replicated dynamics,

$$Z = \mathbb{E}_J \sum_s p_U(s)^2 = \sum_s \langle\langle s^{\otimes 4}|\mathbb{U}|0^{\otimes 4}\rangle\rangle, \tag{17}$$

where $\mathbb{U} = \mathbb{E}[U_t \otimes U_t^* \otimes U_t \otimes U_t^*]$ can be represented by an imaginary-time evolution with a replica Hamiltonian defined in Eq. (7). We identify the circuit to have reached anticoncentration if $Z \approx c2^{-N}$ and to not have anticoncentration if $Z \geqslant e^{N^c} 2^{-N}$ for some $O(1)$ constant c.

In Fig. 2 we study the averaged collision probability in a one-dimensional Brownian circuit by the tensor network simulations. We find that the Brownian circuit anticoncentrates at $\ln N$ depth, which is consistent with the fact that local Haar random circuits anticoncentrate in $\Omega(\ln N)$ depth in one dimension [16]. Furthermore, in Fig. 2(b) we show data collapse that is consistent with the approximate form for the collision probability

$$2^N Z = 2 + c_1 e^{-c_2(t - \tau^* \ln N)} \tag{18}$$

for $O(1)$ constants c_1 and c_2. This expression can be justified by the effective Hamiltonian picture as follows.

Because $\mathbb{U} = e^{-Ht}$, with H given by Eq. (7), it effectively projects the initial state $|0^{\otimes 4}\rangle\rangle$ to the ground state $2^N \mathbb{U}|0^{\otimes 4}\rangle\rangle \approx |\text{id}\rangle\rangle^{\otimes N} + |\text{swap}\rangle\rangle^{\otimes N} + \text{excitations}$. The leading contribution of excitations is given by a single domain wall (since we have used the open boundary condition, a single domain wall is
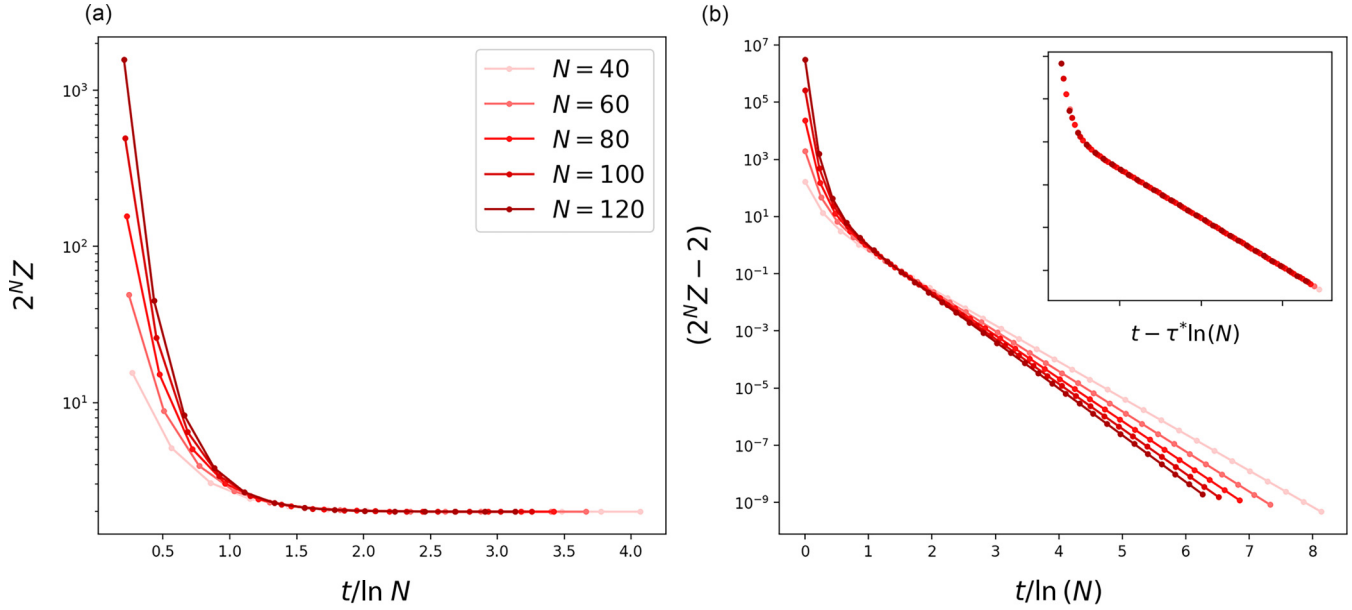
FIG. 2. Anticoncentration in the Brownian circuit: (a) $Z \sim 2^{-N}$ in $t / \ln N = \tau^* \approx 1.5$ time and (b) data collapse, which is consistent with Eq. (18).

allowed), $|DW_k\rangle\rangle \approx |swap\rangle\rangle^{\otimes k} \otimes |id\rangle\rangle^{\otimes(N-k)}$, $k = 1, \ldots, N - 1$. Therefore, the multiplicity of such an excitation is proportional to N. The excitation energy Δ, on the other hand, is a constant independent of N and it contributes to an exponential function $e^{-\Delta t}$. Therefore, according to this picture, the prediction for the collision probability reads

$$2^N Z \approx 2 + N e^{-\Delta t} = 2 + e^{-\Delta[t-(1/\Delta)\ln N]}, \qquad (19)$$

where we note that $\sum_s \langle\langle s|id\rangle\rangle = \sum_s \langle\langle s|swap\rangle\rangle = \sum_s \langle\langle s|DW_k\rangle\rangle = 1$. This result is consistent with the data collapse. In particular, it is clear that the transition time $\ln N$ is due to the entropy of the domain-wall excitation.

B. Hardness of classical simulation of sampling

As a consequence of anticoncentration and randomness, classical simulation of the output probabilities of the Brownian circuits after $\ln N$ depth is expected to be hard. In this section we provide evidence for a transition in (classical) computational hardness, with respect to a particular algorithm for approximate classical simulation, at $t \sim \ln N$ depth.

We study the computational hardness of the patching algorithm introduced in [29,43]. Heuristically, the algorithm attempts to sample from the marginal probability distribution of spatially separated patches and then combine the results together. This succeeds in poly(N) time if the output distribution of the state generated by the circuit has decaying long-range correlations. Without going into the details of the algorithm itself, we study the condition on the long-range correlations for which the algorithm is expected to successfully sample from the output distribution.

Consider a tripartition of N qubits into $A \cup B \cup C$ such that $dist(A, C) \geqslant l$. For the output probability distribution $p_U(s) = |\langle s|U|0\rangle|^2$, we consider the conditional mutual

information between the regions A and C conditioned on B, as in $I(A : C|B)_p = S(AB)_p + S(BC)_p - S(B)_p - S(ABC)_p$, where $S(A)$ refers to the entropy of the marginal distribution of p on the region A. The output distribution is defined to have the $f(l)$ Markov property if $I(A : C|B)_p \leqslant f(l)$. We quote the main theorem about the condition for a successful patching algorithm from [29].

Theorem. The patching algorithm succeeds in poly(N) time to sample from a probability distribution arbitrarily close in total variation distance to the exact output distribution $p_U(s)$ of a quantum circuit on N qubits, if $p_U(s)$ has $e^{-\Omega(l)}$ Markov property, for a suitable choice of the length-scale parameter l.

In the local Brownian circuits introduced earlier, we can directly compute an annealed averaged version of the Rényi-2 version of the conditional mutual information of the output distribution $p_U(x)$, i.e., $I^{(2)}(A : C|B)_p = S^{(2)}_{ann}(AB)_p + S^{(2)}_{ann}(BC)_p - S^{(2)}_{ann}(B)_p - S^{(2)}_{ann}(ABC)_p$, as a function of time t. Here the annealed entropy is defined as $S^{(2)}_{ann}(p) = -\ln \mathbb{E} p^2$.

In Figs. 3(a) and 3(b) we study the annealed Rényi-2 CMI for an equal tripartition of the qubit chain, i.e., $|A| = |B| = |C| = N/3$, and find that there is a transition at $\ln N$ depth. In particular, at long times, $I^{(2)}(A : C|B)_p$ asymptotes to $\ln 2$, indicating long-range correlations in the output probability distribution. At short times, the data are consistent with $I^{(2)}(A : C|B)_p \sim O(e^{-N})$. There is furthermore a sharp transition at $t \sim \tau^* \ln N$ at $\tau^* \approx 1.2$. The data collapse as a function of $t - \tau^* \ln N$ is shown in the inset in Fig. 3(b), indicating the same statistical mechanical interpretation as the collision probability.

We note, however, that the transition in the annealed Rényi-2 version of the CMI does not necessarily imply a transition for the actual $n \to 1$ limit of the exact averaged CMI. With this caveat, our results provide evidence for the transition in computational hardness, at the same depths as the onset of anticoncentration.
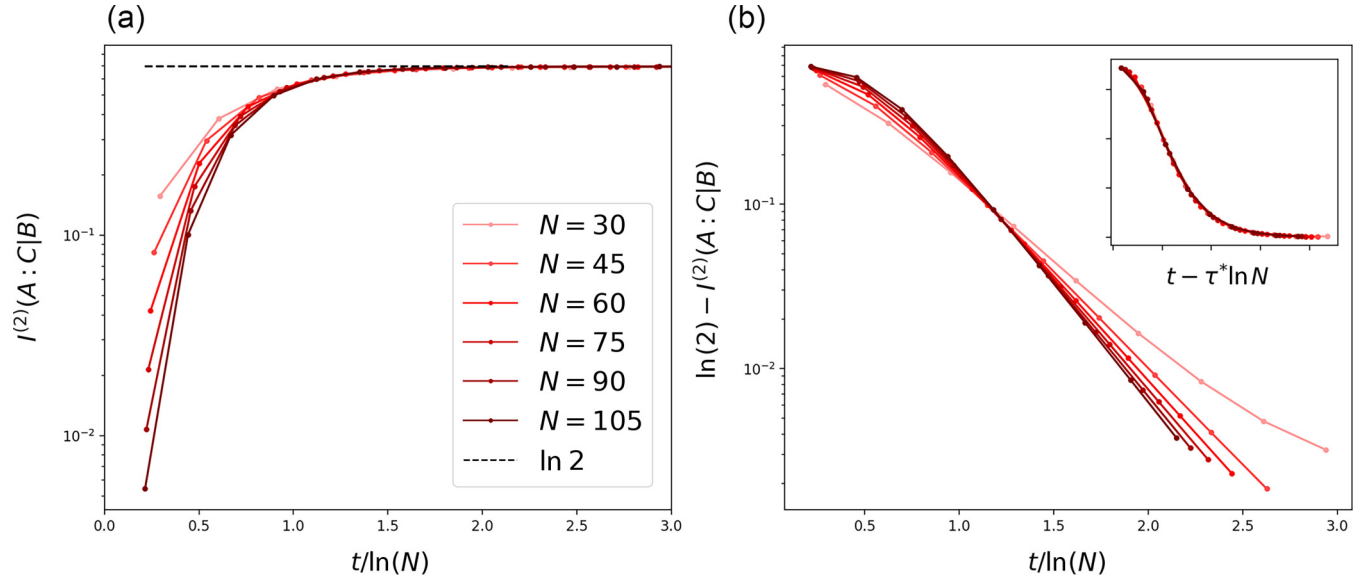
FIG. 3. Phase transition in the annealed Rényi-2 CMI of $p_U(s)$. We consider an equal tripartition of the spin chain such that $|A| = |B| = |C| = N/3$, with B separating regions A and C, and we plot Rényi-2 CMI $I^{(2)}(A : C|B)$. As N is increased, for $t < \tau^* \ln N$ ($\tau^* \approx 1.2$), the CMI decays with N proportionally to e^{-N}. For larger times $t > \tau^* \ln N$ the CMI does not decay with N and asymptotes to $\ln 2$.

IV. NOISY BROWNIAN CIRCUITS

Random circuit sampling is widely implemented in experiments to show quantum advantage. However, sufficiently large noise can diminish the quantum advantage. It was reported recently that there is a noise-induced phase transition in an appropriate quantum-classical benchmark for random circuit sampling [8,31–33]. For weak noise, the cross-entropy benchmarking provides a reliable estimate of fidelity, whereas for strong noise, it fails to accurately reflect fidelity.

A. Cross-entropy benchmarking

In the random circuit sampling, we start from a product state $\rho_0 = |0\rangle^{\otimes N}\langle 0|^{\otimes N}$ (the initial state does not really matter and we choose this just for simplicity) and evolve the state using the Brownian spin Hamiltonian. For brevity, we denote the unitary generated by the Brownian spin model by U. In an ideal case, i.e., there is no noise, the final state is

$$\rho = U \rho_0 U^\dagger. \tag{20}$$

A measurement is performed on the computational basis and this will generate a probability distribution

$$p(s) = \langle s|\rho|s\rangle, \tag{21}$$

where s denotes the bit string.

In a real experiment, the implementation of the Brownian spin Hamiltonian is not ideal because errors can occur. In this case, the time evolution of the system is in general not unitary and should be described by a quantum channel,

$$\rho_{\text{err}} = \mathcal{N}(\rho_0). \tag{22}$$

Here $\mathcal{N}$ denotes the noise channel. The probability distribution for a bit string s is now given by

$$q(s) = \langle s|\rho_{\text{err}}|s\rangle. \tag{23}$$

We are interested in the linear cross-entropy benchmarking, defined as

$$\chi_{\text{XEB}} = 2^N \sum_s p(s)q(s) - 1, \tag{24}$$

where $p(s)$ is an ideal distribution (which in practice can be estimated by classical simulations) and $q(s)$ is the probability distribution sampled from real experiments. Since the circuit involves Brownian variables, we consider the average over these random variables, $\mathbb{E}(\chi_{\text{XEB}})$.

B. XEB in the replica model

Using the operator-state mapping, we obtain

$$\sum_s q(s)p(s) = \sum_s \langle\!\langle s|\mathcal{N} \otimes U \otimes U^*|0\rangle\!\rangle, \tag{25}$$

where U is the unitary generated by the Brownian spin model and $\mathcal{N}$ denotes the channel generated by both the Brownian spin model and the errors. For simplicity, we define $\mathbb{E}[\mathcal{N} \otimes U \otimes U^*] = \mathbb{U}_{\text{err}}$. The initial and final states are the same as in the collision probability. Actually, the collision probability is closely related to the noiseless XEB.

Consider imperfect time evolution due to the presence of quantum errors. To this end, after integrating over the Brownian variable, we arrived at the imaginary-time evolution given by

$$\sum_s \langle\!\langle s|\mathbb{U}_{\text{err}}|0\rangle\!\rangle = \sum_s \langle\!\langle s|e^{-[H+H'(\lambda)]t}|0\rangle\!\rangle, \tag{26}$$

where $H'(\lambda)$ is the perturbation caused by the noise. The example of dephasing and depolarizing channels are given by Eq. (15). The average XEB then reads

$$\mathbb{E}[\chi_{\text{XEB}}] = 2^N \sum_s \langle\!\langle s|e^{-[H+H'(\lambda)]t}|0\rangle\!\rangle - 1. \tag{27}$$

On the other hand, the average fidelity is given by

$$\mathbb{E}[F] = 2^N \langle\!\langle \text{swap}|^{\otimes N} \mathbb{E}[\mathcal{N} \otimes U \otimes U^*]|0\rangle\!\rangle \tag{28}$$

$$= 2^N \langle\!\langle \text{swap}|^{\otimes N} e^{-[H+H'(\lambda)]t}|0\rangle\!\rangle. \tag{29}$$

Comparing it with the XEB, we can see that the difference comes from the final state.

As discussed before, the noise lifts the degeneracy and behaves as an external field. We denote the local Zeeman energy by ϵ. The Zeeman field is a relevant perturbation even in the symmetry-breaking phase. We will show that the competition between one of the lifted ground states and the excited state leads to a first-order transition at a finite noise rate $\epsilon N \sim$ const. We will also perform a finite-size-scaling analysis to verify such a first-order transition in the following.

We consider the evolution of XEB as a function of time. In the long-time limit, we expect the time-evolved state is a superposition of the ground state with a few low-lying excitations. The time-evolved state can be approximately written as

$$2^N \mathbb{U}_{\text{err}}|0^{\otimes 4}\rangle\!\rangle \approx |\text{id}\rangle\!\rangle^{\otimes N} + e^{-N\epsilon t}|\text{swap}\rangle\!\rangle^{\otimes N}$$
$$+ e^{-\Delta t}\sum_k e^{-k\epsilon t}|\text{DW}_k\rangle\!\rangle + \sum_k e^{-(2\Delta+\epsilon)t}|\text{SF}_k\rangle\!\rangle, \tag{30}$$

where Δ is the local energy cost of a domain wall and the ϵ are the local energy cost and the Zeeman energy of a local spin flip. We have included both domain-wall excitations and local spin flips, $|\text{SF}_k\rangle\!\rangle = |\text{id}\rangle\!\rangle^{\otimes k-1} \otimes |\text{swap}\rangle\!\rangle \otimes |\text{id}\rangle\!\rangle^{\otimes N-k}$. Note that the domain-wall excitation can lead to an extensive energy cost, but we need to include it because the external field scales as $\epsilon \sim 1/N$. Therefore, the average XEB at late time is

$$\mathbb{E}[\chi_{\text{XEB}}] = e^{-N\epsilon t} + e^{-\Delta t}\sum_{k=1}^{N-1} e^{-k\epsilon t} + Ne^{-(2\Delta+\epsilon)t}. \tag{31}$$

On the other hand, the average fidelity is

$$\mathbb{E}[F] = e^{-N\epsilon t}. \tag{32}$$

Actually, the fidelity is lower bounded by 2^{-N}. This is because $|\text{id}\rangle\!\rangle^{\otimes N}$ and $|\text{swap}\rangle\!\rangle^{\otimes N}$ are orthogonal only at the thermodynamic limit $N \to \infty$. For a finite N, their overlap is $\langle\!\langle \text{id}|^{\otimes N})(|\text{swap}\rangle\!\rangle^{\otimes N} = 2^{-N}$.

It is clear that for the XEB to well estimate the fidelity, we require $e^{-N\epsilon t} \gg e^{-\Delta t}$. Consider the ratio between them

$$\frac{\mathbb{E}[F]}{\mathbb{E}[\chi_{\text{XEB}}]} \approx \frac{1}{1 + e^{-\Delta t + N\epsilon t}}. \tag{33}$$

To the leading order in N, there is a noise-induced phase transition at $\epsilon_c = \frac{\Delta}{N}$, separating a weak noise phase, where the XEB well estimates the fidelity, and a strong noise phase, where they do not match. This is consistent with the scaling dimension analysis.

C. Noise-induced transition

In the short-time region, all kinds of excitations contribution to the XEB, and its evolution is nonuniversal. A crude
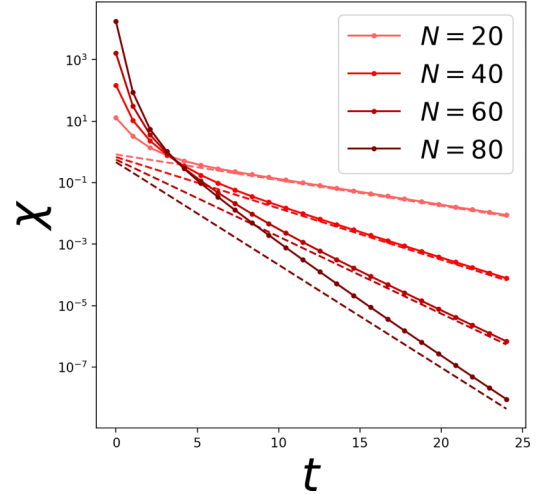

FIG. 4. In the presence of noise, there is a depth-driven crossover at $t^* \sim O(1)$; for $t < t^*$ the linear XEB $\chi \sim e^N$ and for $t > t^*$, $\chi \sim e^{-N\epsilon t}$. We consider a constant noise strength of $\lambda = 0.01$.

estimate of the XEB is given as

$$\mathbb{E}[\chi_{\text{XEB}}] \approx (1 + e^{-(2\Delta+\epsilon)t})^N - 1. \tag{34}$$

This estimate comes from the superposition of all possible spin flips at each site.[3] Here Δ is the effective local energy cost of a spin flip. The XEB is exponential in the system size of approximately $\exp(Ne^{-(2\Delta+\epsilon)t})$, but this behavior decays exponentially fast. Then the XEB will transition to the late-time behavior. In the long-time limit, since we are at the weak-noise phase, we expect the XEB matches fidelity. To verify this, we plot the time evolution of XEB (solid curves) and fidelity (dashed curves) in Fig. 4 for a fixed noise rate. At the long-time limit, their evolution follows closely. The fact that the deviation is larger for a bigger N is because we have fixed ϵ. It is also clear that the XEB curves exhibit a crossover from a short-time nonuniversal region to a long-time universal region.

In order to show the noise-induced phase transition in our replica model, we plot the time evolution of the XEB for different noise rates in Fig. 5(a). It is clear that when the noise rate is less than $\lambda^* \approx 0.84/N$, the XEB tracks the fidelity very well. Here the fidelity is shown by a dashed curve. Note also that the fidelity has a lower bound given by 2^{-N}.

Next, to connect this to the statistical mechanical model and implement a finite-size-scaling analysis, we consider scaling $t \sim N$ to feature an equal space-time scaling. The ratio between the fidelity and XEB is plotted in Fig. 5(b) for different system sizes. The crossing indicates a transition at $\lambda^* N \approx 0.84$. The inset shows data collapse for different sizes as a function of $(\lambda - \lambda^*)N^2$, which shows $1/\nu = 2$.

To understand this exponent, we briefly review the finite-size scaling at first-order phase transitions. The finite-size scaling near a first-order phase transition was studied in

---

[3]For a more accurate estimate, we need to rescale N by a factor $c_3 < 1$. This is because spin flips do not interact with each other only when they are dilute enough.
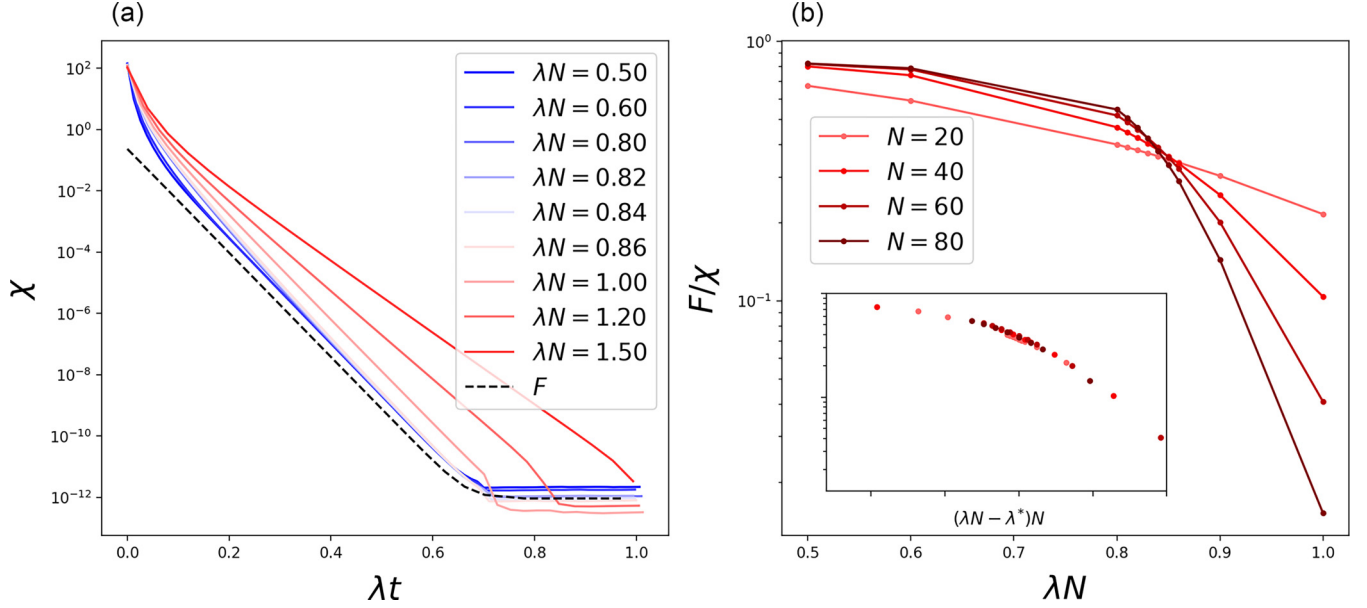
FIG. 5. Noise-driven transition for scaled noise $\lambda \sim c/N$. (a) Plot of χ for $N = 40$ and different values of λN. We find that for $\lambda N \leqslant \lambda^* N \approx 0.84$, χ approximates the fidelity F after an initial fast decay. For $\lambda N > \lambda^* N$, however, χ behaves differently from F, which results in a sharp phase transition as shown in (b) of the order parameter F/χ, evaluated at a time $t > t^* = O(1)$ of initial decay. The scaling collapse is shown in the inset.

Ref. [42]. We briefly repeat the argument here. In a classical Ising model in a d-dimensional cube with size L^d, the probability distribution of the magnetization $P_L(s)$ in the ferromagnetic phase can be well approximated by a double Gaussian distribution

$$P_L(s) \propto e^{-(s-M)^2 L^d/\chi} + e^{-(s+M)^2 L^d/\chi}, \qquad (35)$$

where χ denotes the susceptibility and M is the average magnetization. To incorporate the external field, note that the probability distribution can be expressed as $P_L(s) \propto e^{-fL^d}$, where f is the free-energy density. From the Ising transition, the free energy is given by

$$f = f_0 + \frac{r}{2}s^2 + \frac{u}{4}s^4 - sH \qquad (36)$$

$$= f_0' + \frac{u}{4}(s^2 - M^2)^2 - sH, \qquad (37)$$

where H denotes the external field, $M = \sqrt{-\frac{r}{u}}$ is the average magnetization when $r < 0$, and f_0 and f_0' are unimportant constants. If we approximate the magnetization around $\pm M$, then the double Gaussian distribution reads

$$P_L(s) \propto e^{-[(s-M)^2 - s\chi H]L^d/\chi} + e^{-[(s+M)^2 - s\chi H]L^d/\chi}, \qquad (38)$$

where $\chi = -r$. It is clear that the distribution will be shifted and the one near $s = M$ will be amplified. This probability distribution can serve as a starting point for finite-size-scaling analysis. The external field is equipped with scaling dimension L^{-d}, implying $\nu = 1/d$. Now in our analysis, the Hamiltonian (7) corresponds to a one-dimensional quantum system or a two-dimensional classical Ising model, which leads to $\nu = \frac{1}{2}$, consistent with our scaling data collapse in Fig. 5(b).

D. Hardness of sampling from noisy Brownian circuits

As we have described, the linear cross-entropy benchmark can be described in the two-replica formalism, where the noise acts on only one of the replicas. In this section we briefly comment on the hardness of classical simulation of noisy Brownian circuits, by analyzing the annealed Rényi-2 conditional mutual information of the output distribution $p(s)$ of the noisy circuit, as in Sec. III B. In this formulation the noise acts on both replicas. In Fig. 6 we plot the annealed Rényi-2 CMI as a function of time for two instances of weak and strong scaled local depolarization channels with strength $\lambda = \mu/N$, with $\mu = 0.1, 2.0$, respectively. The plots show that the CMI does not asymptote to $\ln 2$ as the noise-free case and ultimately decays as $e^{-\mu t}$ without any signature of crossing. This suggests that in the long-time limit, even in the presence of scaled noise, the output distribution remains efficiently estimable using the patching algorithm [29].

These numerical results provide evidence that the noise-induced phase transition in the linear cross-entropy benchmark does not signal a phase transition in the hardness of classical simulability of the output distribution of the noisy random circuits. In fact, in the presence of noise, $(1+1)$-dimensional random circuits remain efficiently simulable, i.e., can be efficiently classically sampled from, by the patching algorithm. These results must be taken with the same caveats of annealed versus quenched averages of the CMI that we already provided in Sec. III B.

V. QUANTUM ERROR CORRECTING CODES FROM BROWNIAN CIRCUITS

Random circuits scramble local information into global correlations of a state in a way that is inaccessible to
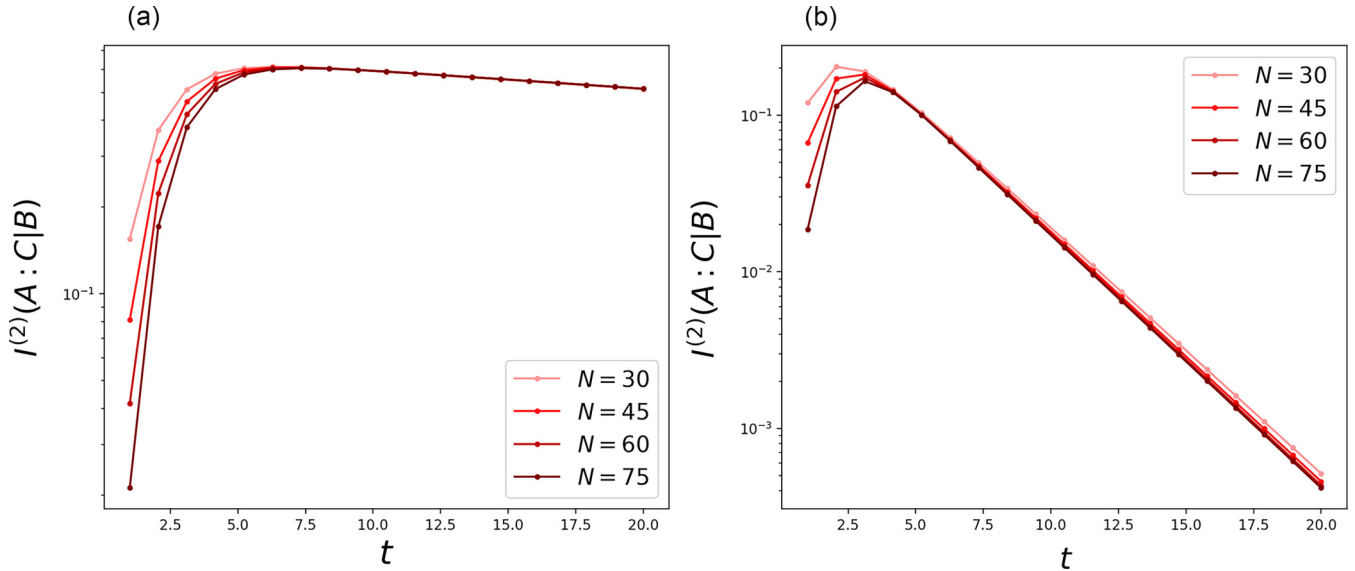
FIG. 6. Dynamics of the annealed Rényi-2 CMI of the classical output distribution of the noisy Brownian circuit for noise levels (a) $\lambda = 0.1/N$ and (b) $\lambda = 2.0/N$.

local probes. As a result of this, the encoded information can be protected from local noise, thereby leading to the notion of random circuits generating quantum error correcting codes [11–13].

A. Decoupling by random circuits

The intuition as to why random circuits are able to dynamically generate a quantum error correcting code comes from the decoupling principle. Consider the setup in Fig. 7, where initial quantum information is initialized in the entangled state between reference R (code subspace) and part of the system $A_1 \subset A$ such that the dimensions match $|R| = |A_1|$. Now A is subjected to an encoding through the random circuit U_{enc}. Suppose a part of the system $A_4 \subset A$ is subjected to a noise channel $\mathcal{N}$. By Stinespring dilation, the noise channel can be identified as a unitary coupling with an environment E, as shown in Fig. 7. If U_{enc} forms an approximate 2-design, the
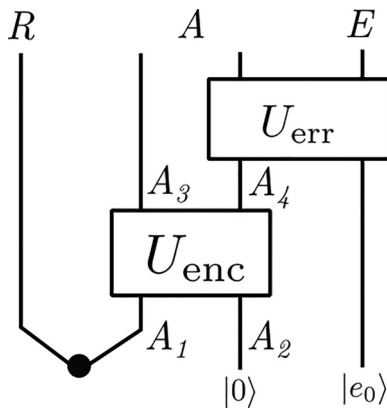

FIG. 7. Unitary encoding U_{enc} of reference R into system A. Any noise in A after the encoding can be represented by a unitary operation U_{err} coupling the part of A where the error acted (A_4 in the figure), with an environment E.

circuit is able to decouple effectively [44], i.e., the environment E has bounded access to the information encoded in R.

Concretely, let us consider local qubit degrees of freedom such that the Hilbert space dimension of any set A is $d_A = 2^{|A|}$. Consider the isometric encoding $V : \mathcal{H}_R \to \mathcal{H}_A$ generated by the circuit U_{enc}, which transforms the basis vectors as

$$|\phi_i\rangle_A \equiv V|i\rangle_R = U_{\text{enc}}|i\rangle_{A_1}|0\rangle_{A_2}. \tag{39}$$

Any density matrix ρ_R of R is encoded as $V\rho_R V^\dagger$. Suppose the encoded state is now subjected to noise, resulting in the density matrix $\rho_{\text{err}} = \mathcal{N}(V\rho_R V^\dagger)$. A convenient probe is the noise-affected encoding of a maximally entangled state between the code subspace R and A_1. By introducing an auxiliary environment E the effect of the noise channel can be represented by a unitary on the combined system and environment $A \cup E$,

$$|\Psi'\rangle = \frac{1}{\sqrt{d_R}} \sum_{i=1}^{d_R} |i\rangle_R U_{\text{err}}(|\phi_i\rangle_A |e_0\rangle_E). \tag{40}$$

Here d_R refers to the Hilbert space dimension for R; if the local degrees of freedom are q-dimensional qudits, then $d_R = q^{|R|}$.

By the decoupling theorem, for U_{enc} that are approximate 2-designs and have small enough error, we have a factorized reduced density matrix on $R \cup E$, $\rho_{RE}^{\Psi'} \approx \rho_R^{\Psi'} \otimes \rho_E^{\Psi'}$. The time required by random circuits with locality to approximately form a 2-design is upper bounded by $O(N^{1/d})$ in d dimensions [17,18]. A probe of the extent of decoupling is the mutual information [37] $I_{\Psi'}(R : E) = S(\rho_R') + S(\rho_E') - S(\rho_{RE}')$.

A central theorem in quantum error correction is the existence of an optimal recovery channel $\mathcal{R}$ that undoes the effect of noise $\mathcal{R}(\rho_{\text{err}}) = \rho_R$ if perfect decoupling has occurred, i.e., $I_{\Psi'}(R : E) = 0$ [37]. This can be generalized to approximate error correction in the presence of approximate decoupling [38,45]. In particular, the trace distance between the recovered state by a near-optimal recovery channel $\mathcal{R}$ and any encoded state can be bounded by the mutual information computed

for Ψ',

$$\|\mathcal{R}(\rho_{\text{err}}) - \rho_R\|_1 \leqslant [I_{\Psi'}(R:E)]^{1/4}. \tag{41}$$

B. Approximate error correction in Brownian circuits

Recently, Ref. [30] derived a bound similar to Eq. (41), with the right-hand side replaced by an entropic quantity different from the mutual information. Mutual information is difficult to analytically study because of the associated replica limit in the definition of the von Neumann entropy. That work instead introduced the mutual purity of the noise-affected state in Eq. (40), which is defined as

$$\mathcal{F}_{\Psi'}(R:E) = \text{Tr}\big(\rho_{\text{RE}}'^2 - \rho_R'^2 \otimes \rho_E'^2\big). \tag{42}$$

Reference [30] showed that for the same approximate recovery channel as in [38], the trace distance between the recovered state and the encoded state can be bounded by the mutual purity

$$\|\mathcal{R}(\rho_{\text{err}}) - \rho_R\|_1 \leqslant d_R^{5/2} d_E^{1/2} [\mathcal{F}_{\Psi'}(R:E)]^{1/4}. \tag{43}$$

We provide a description of the recovery channel and a sketch of the proof of this bound in Appendix 1. This bound can be computed using just a two-replica computation for local Brownian circuits in $1+1$ dimensions with the imaginary TEBD protocol that we have introduced earlier.

C. Numerical results in one dimension

Using the replicated Hilbert space formalism, we can represent the mutual purity for the $(1+1)$-dimensional local Brownian circuit by the expression

$$\mathcal{F}_{\text{RE}}^{\Psi'} = \langle\!\langle\psi_{\text{err}}|\mathbb{U}_{\text{enc}}|\psi_{\text{in}}\rangle\!\rangle = \langle\!\langle\psi_{\text{err}}|e^{-tH_{\text{eff}}}|\psi_{\text{in}}\rangle\!\rangle, \tag{44}$$

where $\mathbb{U}_{\text{enc}} = \mathbb{E}[U_{\text{enc}} \otimes U_{\text{enc}}^\dagger \otimes U_{\text{enc}} \otimes U_{\text{enc}}^\dagger]$, and appropriately defined states $|\psi_{\text{in}}\rangle\!\rangle$ and $|\psi_{\text{err}}\rangle\!\rangle$ in the replicated Hilbert space, given by

$$|\psi_{\text{in}}\rangle\!\rangle = \big(|\text{swap}\rangle\!\rangle - \tfrac{1}{2}|\text{id}\rangle\!\rangle\big)^{\otimes A_1} \otimes |0\rangle\!\rangle^{\otimes A_2}, \tag{45}$$

$$|\psi_{\text{err}}\rangle\!\rangle = 2^N \sum_{m,n=0}^{d_E-1} E_m E_n^* E_n E_m^* |\text{id}\rangle\!\rangle^{\otimes A}. \tag{46}$$

Note that both $|\psi_{\text{in}}\rangle\!\rangle$ and $|\psi_{\text{err}}\rangle\!\rangle$ are not normalized.

The operators E_m are nonunitary operators implementing the error on the systems A,

$$U_{\text{err}}|\psi\rangle_A|e_0\rangle_E = \sum_m E_A^m|\psi\rangle_A|e_m\rangle_E. \tag{47}$$

The derivation is provided in Appendix 2. The replica order of the initial state $|\psi_{\text{in}}\rangle\!\rangle$ reveals that the state breaks the replica symmetry to swap in the region A_1 (reflecting the encoded qubit) and preserves the replica symmetry in A_2. As for the final state $|\psi_{\text{err}}\rangle\!\rangle$, the replica order is id in the region where the error does not act and swap in the region where error acts.

To diagnose the error correcting properties of the Brownian circuit, we need to look at specific noise models. In this section we focus on local depolarization channels acting on a few qubits, say, a fraction p of them. The depolarization channel of strength λ acts on the density matrix as

$$\mathcal{N}_i(\rho) = (1-\lambda)\rho + \frac{\lambda}{3}\left(\sum_{\alpha=x,y,z} \sigma_{i,\alpha}\rho\sigma_{i,\alpha}\right). \tag{48}$$

In Fig. 8(a) we present the plot of the mutual purity of the $(1+1)$-dimensional Brownian circuit as a function of time, where a single qubit in R is encoded in the system A of size N. The noise model is chosen to be the depolarization channel of $\lambda = 0.75$ (erasure noise) acting on a fraction $p = 0.25$ of qubits. It is clear from the plot that the mutual purity initially decays exponentially, until it saturates to the global Haar value, which is $O(2^{-N})$. The time taken for the saturation scales as $t \propto N$. In Appendix 3 we derive the explicit result for mutual purity with globally Haar random encoding $\mathcal{F}_{\text{Haar}} = O(2^{-N})$. This numerical result demonstrates that the Brownian circuit approximates a 2-design in $O(N)$ times, and we show in Fig. 8(b) that the 2-design transition occurs after time $\tau^* N$, where $\tau^* \sim 0.77$. The scaling collapse of the transition reveals that $\mathcal{F}/\mathcal{F}_{\text{Haar}} \sim f(t - \tau^* N)$.

Furthermore, we can study the mutual purity and the right-hand side (RHS) of the quantum error correction bound (43) for different values of p. In Fig. 8(d) we plot the saturation value of the RHS of Eq. (43) (after the Brownian circuit has run for $t = N$ steps) for different values of p and system sizes N, for a single-qubit encoding, and for a depolarization channel of strength $\lambda = 0.75$. We find that the RHS of the error correction bound undergoes a transition at $p^* \approx 0.17$, which provides a lower bound to the threshold of this quantum error correction code. Note the quantum error correction bound in Eq. (43) guarantees that for $p < p^*$ the Brownian circuit generates a quantum error correction code whose errors are correctable using the recovery channel outlined in Appendix 1.

We do not expect this threshold to be tight, as the error correction bound with the mutual purity is expected to be looser than the bound from mutual information. However, the numerical results strongly indicate that both the quantum error correction transition with t, the depth in the Brownian circuit (the time when the circuit approximates a 2-design), and the threshold transition correspond to a first-order domain-wall pinning transition.

D. Coding transitions

As discussed in the preceding section, the mutual purity is given by the amplitude $\mathcal{F}_{\text{RE}}^{\Psi'} = \langle\!\langle\psi_{\text{err}}|\mathbb{U}_{\text{enc}}|\psi_{\text{in}}\rangle\!\rangle$. It is convenient to view the space-time layout of the Brownian circuit as a two-dimensional statistical model. In our setting, this is nothing but the mapping from a d-dimensional quantum system to a $(d+1)$-dimensional classical system. It is important to note that in the wave function $|\psi_{\text{in}}\rangle\!\rangle$, the encoded $|A_1|$ qubit is mapped to a projection to $|\text{swap}\rangle\!\rangle$, i.e.,

$$\langle\!\langle\text{id}|\big(|\text{swap}\rangle\!\rangle - \tfrac{1}{2}|\text{id}\rangle\!\rangle\big) = 0, \tag{49}$$

whereas the wave function of the rest $|A_2|$ qubits behaves as a free-boundary condition, i.e., $\langle\!\langle\text{id}|0000\rangle\!\rangle = \langle\!\langle\text{swap}|0000\rangle\!\rangle = \tfrac{1}{2}$.

On the other hand, $|\psi_{\text{err}}\rangle\!\rangle$ can effectively change the boundary condition on the top layer. In particular, for the
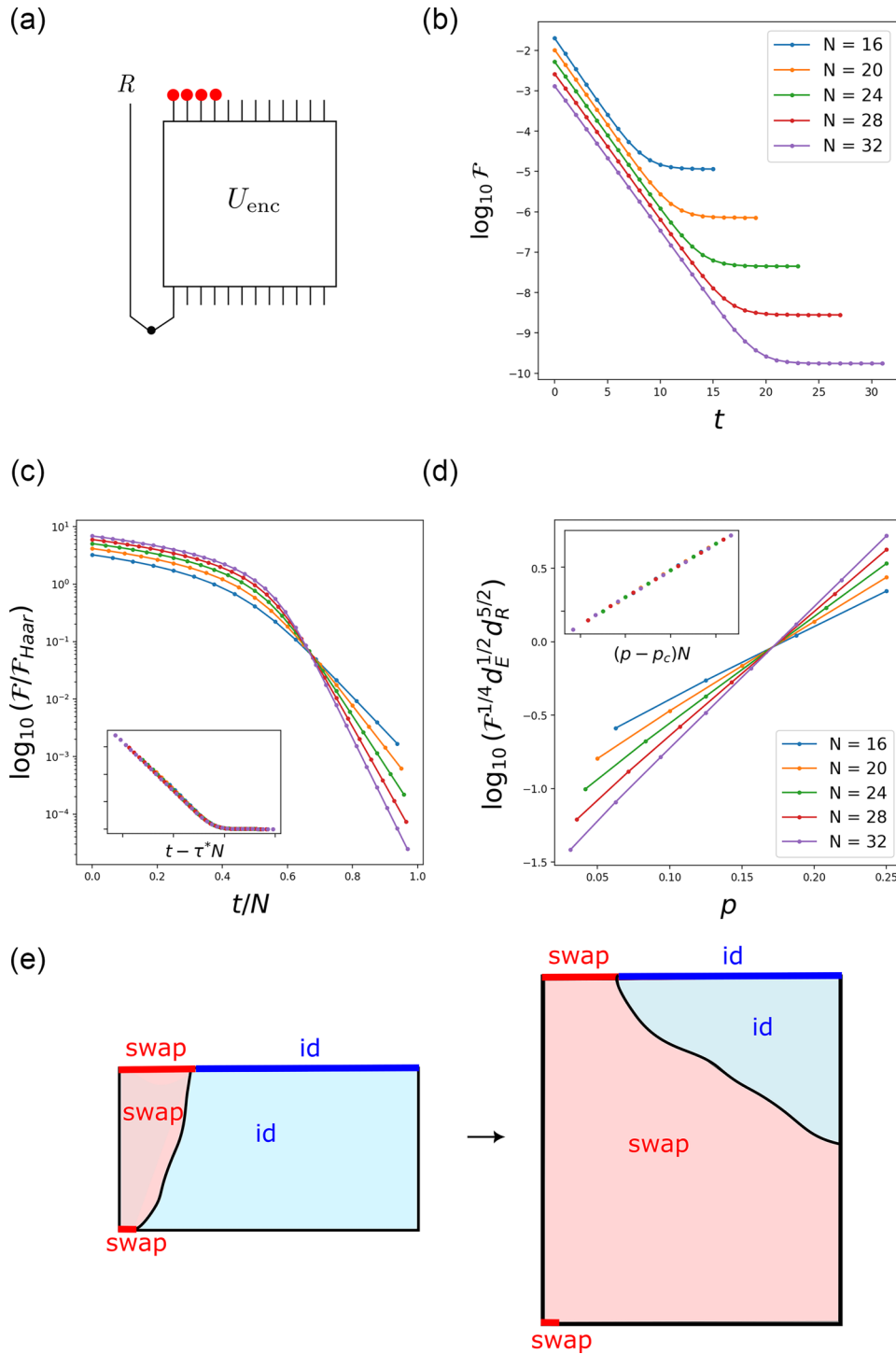
FIG. 8. The 2-design transition in the Brownian circuit. (a) We encode one qubit on the left end and have erasures (depolarization channel of strength $\lambda = 0.75$) act on a fraction p of qubits on the left of the chain. (b) Mutual purity for the setup in (a) with $p = 0.25$, plotted as a function of time. (c) Here $\mathcal{F}$ saturates to $\mathcal{F}_{\text{Haar}} \approx O(2^{-N})$ after $t \sim O(N)$ time. We scale the time linearly with N and find that there is a transition at $t = \tau^* N$, with $\tau^* \approx 0.77$. The scaling collapse of this transition is shown in the inset. (d) Plot of the right-hand side of the error correction bound of Eq. (43) for different values p, with the saturated mutual purity after $t \sim N$ time of encoding by the Brownian circuit. There is a transition $p_c \approx 0.17$ below which the error is correctable and can thus be identified as a lower bound to the true error threshold of the code. The scaling collapse of this transition is shown in the inset. (e) Transition in the mutual purity can be related to a first-order pinning transition between two domain-wall configurations separating domains of two ordered states consistent with the boundary conditions set by the definition of mutual purity. As described in the text, the trace structure in the definition of mutual purity forces the boundary state to certain ordered states. In the initial-time boundary, the state is swap ordered in the part where the reference qubit is encoded (red) and has the free-boundary condition elsewhere (no ordered state). The timelike boundaries on the left and right are also free by the open-boundary condition. In the final state, the swap (red) part refers to the erasure errors and the id (blue) part refers to the partial trace in the definition of mutual purity.
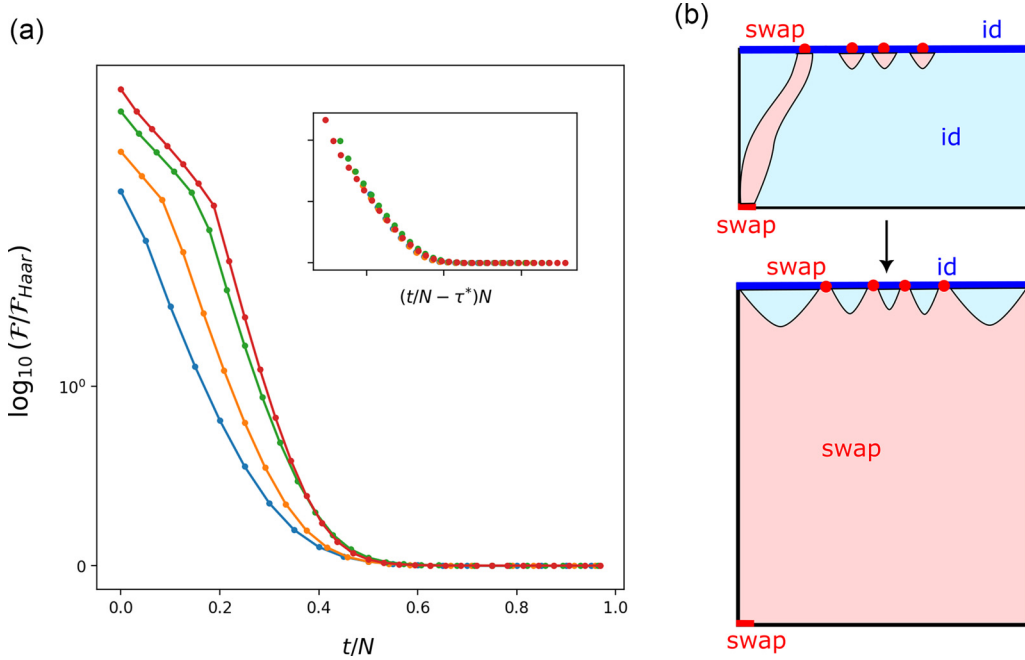
FIG. 9. Mutual purity with erasures of a fraction $p = 0.25$ of qubits on random locations. The data presented are averaged over 80 and 20 random instances of the erasure locations for $N = 20, 24, 28$ and $N = 32$ chains.

single-qubit depolarization channel at site i, the wave function becomes a superposition of two spins

$$|\psi_{\text{err},i}\rangle\rangle = \left(1 - \tfrac{4}{3}\lambda\right)^2 |\text{id}\rangle\rangle + \tfrac{4}{3}\lambda\left(1 - \tfrac{2}{3}\lambda\right)|\text{swap}\rangle\rangle. \quad (50)$$

Note that when $\lambda = \tfrac{3}{4}$, the wave function is given by $|\text{swap}\rangle\rangle$ only. Therefore, the statistical mechanical picture is that in the symmetry-breaking phase of the Ising model, the boundary condition caused by the noise channel $|\psi_{\text{err}}\rangle\rangle$ will induce different domains in the bulk, namely, these are domains denoted by either id or swap (equivalently, the two Ising values) as shown schematically in Fig. 8(e). The mutual purity is only nonzero when the encoded qubit is located in the swap domain.

To better understand the coding transition, we perform a finite-scaling analysis of mutual purity as a function of depth and discuss different cases in the following.

Noisy region overlaps the encoding qubit. As shown in Fig. 8(a), the reference qubit is encoded on the leftmost edge and the noise occurs in a contiguous region that is also on the left edge. In this case, there are many domain-wall configurations that can contribute to the mutual purity. To simplify the discussion, we focus on two different domain walls: One ends on the bottom layer and the other ends on the right edge. A schematic plot of these two domain walls is shown in Fig. 8(e). It is clear that their contributions are

$$\mathcal{F} \sim e^{-\Delta t} + e^{-\Delta'(1-p)L} \quad (51)$$

$$= e^{-\Delta'(1-p)L}(1 + e^{-\Delta t + \Delta'(1-p)L}), \quad (52)$$

where Δ and Δ' denote the tension of the two kinds of domain walls, respectively, and L is the length of the chain. In the short-time region, the first kind of domain wall dominates, while in the long-time region, the second kind of domain wall

dominates and it becomes time independent. There is an exchange of dominating domain configurations, as demonstrated in Fig. 8(e). The transition time is roughly $\frac{\Delta'(1-p)}{\Delta}L \propto N$. This explains the behavior in Figs. 8(b) and 8(c). Replacing the contribution from the second kind of domain wall by $\mathcal{F}_{\text{Haar}}$, we can obtain $\mathcal{F}/\mathcal{F}_{\text{Haar}} = 1 + e^{-(\Delta t + \ln \mathcal{F}_{\text{Haar}})}$, which is consistent with the data collapse performed in Fig. 8(c).

Random noisy region. In this case, the noise occurs in random positions, as shown in Fig. 9. The picture of exchange of two kinds of domain-wall configuration is still correct. The inset of Fig. 9 shows consistent data collapse.

Noisy region does not overlap the encoding qubit. The encoding qubit and the noisy region are shown in Fig. 10. In the calculation, we set $\lambda = \tfrac{3}{4}$. The boundary condition creates a domain wall at the boundary between the noisy qubits and the noiseless qubits. Due to the causality, the backpropagation of the domain wall is constrained in an emergent light cone. Thus, the mutual purity is zero (up to an exponentially small number of N) when the encoding qubit is still outside the backpropagating light cone of the domain wall. Moreover, unlike in the previous case where the first kind of domain wall that ends on the bottom can lead to a finite mutual purity, here, only the second kind of domain wall that ends on the right boundary can have a significant contribution to the mutual purity. This is only possible when the backpropagating light cone hits the right boundary. Therefore, this indicates a dynamical transition at a timescale that is proportional to the system size. In Fig. 10 the crossing of mutual parity in different sizes indicates such a transition.

We also performed the data collapse in the inset of Fig. 10. Different from the previous two cases, the scaling is given by $(t - \tau^* N)/\sqrt{N}$. To understand this, note that the id domain backpropagates to the light cone as shown in Fig. 10(c). In the symmetry-breaking phase, the domain wall can fluctuate away
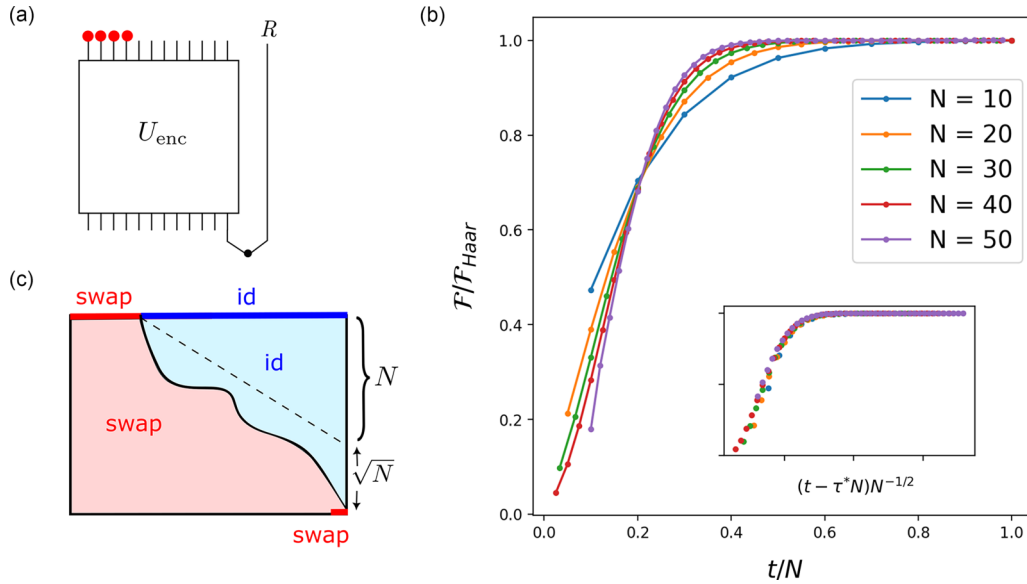
FIG. 10. (a) Single-qubit reference encoded on the right end of chain and erasures of a fraction $p = 0.25$ of qubits on the left of chain. Only (c) a specific domain-wall configuration contributes to the mutual purity dynamics as plotted in (b).

from the light cone.[4] The average position is $\sqrt{N}$ away from the domain wall [46]. Furthermore, the fluctuation of the domain wall is captured by a universal function of $\alpha = \delta L/\sqrt{N}$ [46], where δL denotes the distance away from the light cone. More concretely, the magnetization profile is a function of α at the distance that is of the order $\sqrt{N}$ (outside this distance, the magnetization is given by either one of the two spin polarizations). We expect that this function also captures the mutual purity as the latter also probes the swap spin at the right boundary. Now, since the light cone reaches the right boundary at a time of order N, the mutual purity is then a universal function of $(t - \frac{N}{v})/\sqrt{N}$, where v is the light speed. This explains the data collapse.

In summary, depending on whether the noise occurs in the encoding qubit, we discover distinct coding transitions in mutual purity. If the noisy region covers the encoding qubit, there are two kinds of domain-wall configurations contributing to the mutual purity. They are schematically shown in Fig. 8(e). The exchange of dominance between the two kinds of domain walls underlies the physics of the coding transition in this situation. On the other hand, if the noisy region does not cover the encoding qubit, the mutual purity is only nonzero when the noise backpropagates to the encoding qubit. In this case, the transition is induced by the fluctuating domain walls and captured by a different scaling $N^{-1/2}$, as shown in the data collapse.

We note that there have been many recent works on characterizing the dynamically generated quantum error correcting codes arising from hybrid RQCs with measurements and dissipation, where similar statistical mechanical mappings have been used [47–49]. However, in this work we are studying the purely unitary case and also focus on a particular two-replica quantity named the mutual purity, which bounds the error correction properties of the circuit, without requiring the replica limit. In studying the coding transitions, we have considered the purely unitary encoding using a RQC and explored its coding properties. An interesting direction of work is studying the effects of dissipation in the encoding process itself, which has recently been studied in [49,50].

An important question is examining the nature of coding phase transitions. As explored in [48], the transition in mutual information in hybrid circuit encoding (unitaries with measurements) satisfies the critical properties of a directed polymer in a random environment. In RQC encodings with boundary dissipation, the transition in quenched quantities also has the criticality of pinning-depinning transitions in directed polymers [49]. In that regard, the results of the transition in mutual purity in our work instead satisfy Ising-like transitions, corresponding to annealed mutual-information-like quantities. However, remarkably, such an annealed two-replica quantity, namely, the mutual information, actually bounds the error correction and the approximate recovery inequality in Eq. (43) and is thus a physically relevant informational quantity whose transitions can be identified with Ising-like criticality.

VI. CONCLUSION

In this paper we have used the effective replica Hamiltonian mapping for local Brownian circuits to probe timescales of complexity growth in random quantum circuits, namely, anticoncentration and approximate unitary-design generation. The effective replica model serves two purposes. First, we can perform large-scale numerics to simulate several quantum informational quantities for long times, using tensor network

---

[4]Note that in the symmetry-breaking phase, there are still two phases for domain walls, the pinning and depinning phases, separated by a pinning transition. For our case, since the coupling at the top layer is the same as the coupling in the bulk, the depinning transition is the same as the symmetry-breaking transition. This means the domain wall is depinned and can fluctuate.

tools. This makes local Brownian circuits efficient numerical tools to study unitary quantum many-body dynamics. Second, the model transforms the question of timescales in the real-time dynamics into questions of energy scales in a corresponding thermodynamic problem, which allows us to make analytical progress.

We have shown that local Brownian circuits in $1 + 1$ dimensions anticoncentrate in $\ln N$ time, consistent with earlier results in local Haar random circuits [16]. Furthermore, we have analyzed the success condition of an approximate classical algorithm [29] to sample from the output distribution of Brownian circuits and have identified that there is evidence of a sharp transition in the computational hardness of simulation at the same timescale. The anticoncentration transition arises from the transition in dominance of different low-energy states of the effective Hamiltonian in the collision probability. In particular, the collision probability (a probe of anticoncentration) gets a contribution from eigenstates of the effective Hamiltonian with domain walls and the timescale where this becomes relevant can be related to the logarithm of the number of such domain-wall states (which in one dimension is approximately N).

In the presence of noise, we showed that there is a noise-induced phase transition in the linear cross-entropy benchmark χ_{XEB}, as has been recently demonstrated for related noisy random circuit models in [8,31]. This can be seen as a consequence of explicit replica symmetry breaking in the effective Hamiltonian model in the presence of noise acting on a single replica of the system. By relating the χ_{XEB} to specific transition amplitudes in the corresponding replica model, we identify the noise-induced transition in the cross-entropy benchmarking as the transition in the dominance of certain domain-wall states in the presence of an explicit bulk symmetry-breaking field. The critical properties of the transition can be related to those of external field-induced first-order transitions in the classical Ising model in two dimensions [42].

Finally, we probed the generation of approximate unitary design by Brownian circuits. By directly probing the quantum error correcting properties of the Brownian circuit, namely, a two-replica quantity called mutual purity [30], we found that the $(1 + 1)$-dimensional Brownian circuits become good quantum error correcting codes in $O(N)$ time. This transition can be identified as first-order transitions between certain space-time domain-wall configurations, which are related to first-order boundary-driven pinning transitions in classical Ising models.

There can be several avenues of future research based on this work. Here we have demonstrated $(1 + 1)$-dimensional Brownian circuits as a useful numerically accessible tool for studying the dynamics of quantum information. A natural question is whether the same numerical feasibility extends to higher dimensions. Here we speculated on the dynamics and transitions in informational quantities in higher-dimensional Brownian circuits $d > 1$ (here d is the spatial dimension of the Brownian circuit, N is total number of qubits, and we also used the volume $L^d \sim N$, with L the length scale).

Collision probability. It is still true that in higher dimensions, the collision probability at long enough time is dominated by two grounds states and elementary excitations. Distinct from the situation in one dimension, now the lowest excitation is given by local spin flips with an energy that is independent of system sizes. Nevertheless, the entropy of such a local excitation is proportional to the system size N. Therefore, we expect that the Brownian circuit anticoncentrates on a $\ln N$ timescale, similar to that in one dimension [16].

Computational transition in the patching algorithm. The patching algorithm is closely related to the symmetry breaking of the underlying two-replica spin model [29]. In higher dimensions $d > 1$, the discrete symmetry can be broken in a finite depth. This contrasts with the one-dimensional case, where even the discrete symmetry can only be broken in a logarithmic depth. This means that the patching algorithm will fail when the depth of the Brownian circuit exceeds a critical depth that is independent of system sizes.

Noisy cross-entropy benchmarking. A noise ϵ behaves as an external field and will lift the degeneracy between $|id\rangle\!\rangle$ and $|swap\rangle\!\rangle$, i.e., $|swap\rangle\!\rangle$ will be suppressed by a factor of $e^{-N\epsilon t}$. On the other hand, as discussed in the collision probability, the elementary excitation is given by local spin flips. With an external field, there is an additional cost, adding up to a factor of approximately $e^{-z\Delta t - \epsilon t}$, where z is the coordination number. Therefore, we expect that when the noise rate scales as $1/N = 1/L^d$, there will be a first-order phase transition with critical exponent given by $1/\nu = d + 1$.

Coding transition. The dynamical transition for the Brownian circuit to achieve an approximate unitary 2-design is given by the transition of dominance between two kinds of domain walls. It should be the same in higher dimensions. Therefore, the transition occurs on a timescale of approximately $L = N^{1/d}$ [18]. Next consider the different regions of noise and the encoding qubit. We expect that the mutual purity transition is similarly given by transitions of domain walls when the noisy region overlaps the encoding qubit. On the other hand, when the noisy region does not overlap the encoding qubit, we expect that the fluctuation of domain wall dictates the coding transition.

Even in $1 + 1$ dimensions, this work paves the way for exploration of quantum information dynamics in symmetric Brownian circuits, by studying directly the spectrum of the effective Hamiltonian in the presence of other circuit symmetries. Another direction of interest is incorporating the effects of mid-circuit measurements in the entanglement dynamics in Brownian circuit [28,51].

In this work we have focused on only two-replica quantities, such as collision probabilities and mutual purities. In principle, any integer k replica quantities can be represented in the effective Hamiltonian picture, with q^k local Hilbert space dimension (q being the dimension of the original degrees of freedom), which makes numerical methods intractable at large sizes for large k. An outstanding question is to develop controlled numerical methods or analytical techniques to take the $k \to 1$ replica limit.

for the tensor network simulations [41]. The numerical simulations were performed using the Symmetry HPC system at Perimeter Institute (PI). Research at PI was supported in part by the government of Canada through the Department of Innovation, Science and Economic Development and by the Province of Ontario through the Ministry of Colleges and Universities. S.-K.J. was supported by a startup fund at Tulane University.

APPENDIX: QUANTUM ERROR CORRECTING CODES GENERATED BY BROWNIAN CIRCUITS

1. Error correction bound with mutual purity

In this Appendix we briefly recap the derivation of the error correction bound (43) in the main text, which was derived in [30]. We assume the setup described in Fig. 7. Consider first the encoding of the maximally entangled state between the reference R and system A,

$$|\Psi\rangle_{RA} = \frac{1}{\sqrt{d_R}} \sum_{i=1}^{d_R} |i\rangle_R |\phi_i\rangle_A, \qquad (A1)$$

before any application of error. After the error channel acts on A, we get the noise-affected state on RAE,

$$|\Psi'\rangle_{RAE} = \frac{1}{\sqrt{d_R}} \sum_{i=1}^{d_R} |i\rangle_R U_{\text{err}}(|\phi_i\rangle_A |e_0\rangle_E). \qquad (A2')$$

The error recovery procedure $\mathcal{R}$ [30,38] works by first measuring A using an ideal projective measurement that probes the effect of error in $|\Psi'\rangle_{RAE}$, followed by a unitary update of the state to restore it to $|\Psi\rangle_{RA}$. We first introduce an orthonormal basis of states in A, $|\phi_{ij}\rangle_A$. The projective measurement is given by the projection operators,

$$\Pi_j = \sum_{i=1}^{d_R} |\phi_{ij}\rangle_A \langle \phi_{ij}|_A. \qquad (A2)$$

Depending on the measurement outcome, a corrective unitary $U_{j,A}$ is applied on system A. In order to study the effectiveness of the recovery channel, we want to study the trace distance between the recovered state and the encoded state, $\|\mathcal{R}(|\Psi'\rangle\langle\Psi'|), |\Psi\rangle\langle\Psi|\|_1$. In order to bound this, we introduce a fictitious state $|\tilde{\Psi}\rangle_{RAE}$, which aids in the analysis.

Consider $\tilde{\rho}_{RE} = \rho'_R \otimes \rho'_E$, where the reduced density matrices ρ' are obtained from the state $|\Psi'\rangle_{RAE}$. We now take the fictitious state $|\tilde{\Psi}\rangle_{RAE}$, which is a purification of $\tilde{\rho}_{RE}$ such that the trace distance between $|\tilde{\Psi}\rangle_{RAE}$ and $|\Psi'\rangle_{RAE}$ is minimal. This uniquely defines

$$|\tilde{\Psi}\rangle_{RAE} = \frac{1}{\sqrt{d_R}} \sum_{i=1}^{d_R} \sum_{j=1}^{d_E} \sqrt{\alpha_j} |i\rangle_R |\phi_{ij}\rangle_A |e_j\rangle_E. \qquad (A3)$$

Imagine we apply the recovery channel $\mathcal{R}$ on $|\tilde{\Psi}\rangle_{RAE}$ instead. After the measurement, say the outcome j is obtained. The measured fictitious state is now

$$|\tilde{\Psi}\rangle_{RAE}^j = \frac{1}{\sqrt{d_R}} \sum_{i=1}^{d_R} |i\rangle_R |\phi_{ij}\rangle_A |e_j\rangle_E. \qquad (A4)$$

We can now choose U_j acting on A such that $U_{j,A}|\phi_{ij}\rangle_A = |\phi_i\rangle_A$ and we get

$$U_{j,A}|\tilde{\Psi}\rangle_{RAE}^j = |\Psi\rangle_{RA}|e_j\rangle_E. \qquad (A5)$$

From the above relation we find that

$$
\begin{aligned}
&\|\mathcal{R}(|\Psi'\rangle\langle\Psi'|), |\Psi\rangle\langle\Psi|\|_1 \\
&= \|\mathcal{R}(|\Psi'\rangle\langle\Psi'|), \mathcal{R}(|\tilde{\Psi}\rangle\langle\tilde{\Psi}|)\|_1 \\
&\leqslant \||\Psi'\rangle\langle\Psi'|, |\tilde{\Psi}\rangle\langle\tilde{\Psi}|\|_1,
\end{aligned} \qquad (A6)
$$

where the last inequality follows from the monotonicity property of the trace distance. In [30], the last expression is bounded by the mutual purity defined in Eq. (A13).[5] We quote the result in Eq. (43).

2. Replica computation of mutual purity

We first represent the reduced density matrix of the noise-affected state defined in Eq. (40),

$$
\begin{aligned}
\rho'_{\text{RE}} &= \text{Tr}_A |\Psi'\rangle\langle\Psi'| \\
&= \frac{1}{d_R} \sum_{i,j=1}^{d_R} |i\rangle\langle j|_R \otimes \text{Tr}_A\{U_{\text{err}}[U_{\text{enc}}(|i\rangle\langle j|_{A_1} \\
&\quad \otimes |0\rangle\langle 0|_{A_2})U_{\text{enc}}^\dagger \otimes |e_0\rangle\langle e_0|]U_{\text{err}}^\dagger\}.
\end{aligned} \qquad (A7)
$$

The effect of the U_{err} on the system and the environment can be represented by Kraus operators acting on the system itself,

$$U_{\text{err}}|\psi\rangle_A|e_0\rangle_E = \sum_m E_A^m |\psi\rangle_A |e_m\rangle_E,$$

$$E_A^m : \mathcal{H}_A \to \mathcal{H}_A, \qquad \sum_m E_A^{m\dagger} E_A^m = \mathbf{1}_A. \qquad (A8)$$

The squared density matrix $\rho_{\text{RE}}'^{\otimes 2}$ can be represented by a state vector in the replicated Hilbert space $\mathcal{H} \otimes \mathcal{H}^* \otimes \mathcal{H} \otimes \mathcal{H}^*$ and the replicated unitaries $\mathbb{U}_{\text{enc}} = U_{\text{enc}} \otimes U_{\text{enc}}^* \otimes U_{\text{enc}} \otimes U_{\text{enc}}^*$ and $\mathbb{U}_{\text{err}} = U_{\text{err}} \otimes U_{\text{err}}^* \otimes U_{\text{err}} \otimes U_{\text{err}}^*$ as

$$
\begin{aligned}
|\rho_{\text{RE}}'^{\otimes 2}\rangle\!\rangle &= \frac{1}{d_R^2} \sum_{i,j,i',j'=1}^{d_R} |iji'j'\rangle\!\rangle_R \sum_{s,k=1}^{d_A} \langle\!\langle sskk|_A \mathbb{U}_{\text{err}} \\
&\quad \otimes \mathbb{U}_{\text{enc}}|iji'j'\rangle\!\rangle_{A_1} |0^{\otimes 4|A_2}\rangle\!\rangle_{A_2} |e_0^{\otimes 4}\rangle\!\rangle_E.
\end{aligned} \qquad (A9)
$$

While this representation looks cumbersome, it makes further computations straightforward. The mutual purity is given by $\mathcal{F}_{\text{RE}}^{\Psi'} = \text{Tr}\rho_{\text{RE}}'^2 - \text{Tr}\rho_R'^2\text{Tr}\rho_E'^2$. Let us compute each term.

It is convenient to express Eq. (A9) pictorially, with rank-4 tensors for each subsystem, representing $\mathcal{H} \otimes \mathcal{H}^* \otimes \mathcal{H} \otimes \mathcal{H}^*$,

By unitarity of U_{err} and U_{enc} we have

---

[5]See Appendix B in [30].

Using this result, we find

$$Tr\rho_R'^2 = \frac{1}{d_R^2} \quad = \frac{1}{d_R^2} \quad = \frac{1}{d_R^2} \quad = \frac{1}{d_R} \tag{A10}$$

$$Tr\rho_{RE}'^2 = \frac{1}{d_R^2} \quad ; \quad Tr\rho_E'^2 = \frac{1}{d_R^2}$$

In general, $d_R = 2^{|A_2|}$, where the local Hilbert space dimension is 2. We introduce notation for the following states in the replicated Hilbert space on A:

$$|\psi_{\text{in}}\rangle\!\rangle = (|\text{swap}\rangle\!\rangle - \tfrac{1}{2}|\text{id}\rangle\!\rangle)^{\otimes A_1} \otimes |0000\rangle\!\rangle^{\otimes A_2}, \tag{A11}$$

$$|\psi_{\text{err}}\rangle\!\rangle = 2^N \sum_{m,n=0}^{d_E-1} E_m E_n^* E_n E_m^* |\text{id}\rangle\!\rangle^{\otimes A}. \tag{A12}$$

Note that $|\psi_{\text{err}}\rangle\!\rangle$ is an unnormalized state and the expression for $|\psi_{\text{err}}\rangle\!\rangle$ includes the case for no error acting on the subsystem $A_3 \subset A$ by choosing $E_m = \mathbf{1}_{A_3} \otimes E_{m,A_4}$. Combining all the expressions, the mutual purity is given by

$$\mathcal{F}_{\text{RE}}^{\Psi'} = \langle\!\langle\psi_{\text{err}}|\mathbb{U}_{\text{enc}}|\psi_{\text{in}}\rangle\!\rangle. \tag{A13}$$

The noise model for probing the extent of error correction enters the computation of mutual purity only in the definition of $|\psi_{\text{err}}\rangle\!\rangle$. Consider the local depolarization channel of strength λ on a subset $A_4 \subset A$ such that number of qubits undergoing noise is $|A_4| = p|A|$. The Kraus operators for the depolarization channel are

$$E_0 = \sqrt{1-\lambda}\mathbf{1}, \quad E_{x,y,z} = \sqrt{\frac{\lambda}{3}}\sigma_{x,y,z}. \tag{A14}$$

The local depolarization channel acting on each qubit can be purified using an environmental degree of freedom with four levels 0, x, y, and z. The corresponding $d_{\text{env}} = 4^{p|A|}$.

3. Maximal complexity encoding by Haar random circuits

We can compute the mutual purity for any noise model for an encoding unitary U_{enc} which is a global Haar random unitary. Any unitary 2-designs will exhibit this value of mutual

purity. By examining the time required for the Brownian circuit to achieve this value of mutual purity, we can diagnose the time required for the Brownian circuit to realize a 2-design.

For a global Haar random unitary, we have

$$U_{\text{Haar}} \otimes U_{\text{Haar}}^* \otimes U_{\text{Haar}} \otimes U_{\text{Haar}}^*$$
$$= \frac{1}{d^2-1}\bigg(|\text{id}\rangle\!\rangle\langle\!\langle\text{id}| + |\text{swap}\rangle\!\rangle\langle\!\langle\text{swap}|$$
$$- \frac{1}{d}(|\text{id}\rangle\!\rangle\langle\!\langle\text{swap}| + |\text{swap}\rangle\!\rangle\langle\!\langle\text{id}|)\bigg). \tag{A15}$$

Using this identity for U_{enc} in Eq. (A13), we get the terms in the expression for mutual purity,

$$\mathbb{E}\big[\text{Tr}\rho_{\text{RE}}^2\big] = \left(\frac{1}{\sqrt{d_R}}\right)^4 \frac{1}{d_A^2-1}\bigg(f_{\text{id}}(\lambda)d_R$$
$$+ f_{\text{swap}}(\lambda)d_R^2 - \frac{1}{d_A}\big[f_{\text{id}}(\lambda)d_R^2 + f_{\text{swap}}(\lambda)d_R\big]\bigg),$$

$$\mathbb{E}\big[\text{Tr}\rho_E^2\big] = \left(\frac{1}{\sqrt{d_R}}\right)^4 \frac{1}{d_A^2-1}\bigg(f_{\text{id}}(\lambda)d_R^2$$
$$+ f_{\text{swap}}(\lambda)d_R - \frac{1}{d_A}\big[f_{\text{id}}(\lambda)d_R + f_{\text{swap}}(\lambda)d_R^2\big]\bigg),$$

where we have introduced the notation

$$f_{\text{id}}(\lambda) = \langle\!\langle\psi_{\text{err}}|\text{id}\rangle\!\rangle, \quad f_{\text{swap}}(\lambda) = \langle\!\langle\psi_{\text{err}}|\text{swap}\rangle\!\rangle.$$

Combining the results, we get

$$\mathcal{F}_{\text{RE}}^{\text{Haar}} = \frac{1}{d_A^2-1}\left(1 - \frac{1}{d_R^2}\right)\left(f_{\text{swap}} - \frac{1}{d_A}f_{\text{id}}\right). \tag{A16}$$

For the depolarization channel of strength λ acting on a fraction p of the qubits, we get the expression

$$\mathcal{F}_{\text{RE}}^{\text{Haar}} = \frac{d_A}{d_A^2-1}\left(1 - \frac{1}{d_R^2}\right)[1 - g(\lambda)^{p|A|}], \tag{A17}$$

$$g(\lambda) = (1-\lambda)^2 + \frac{\lambda^2}{3}. \tag{A18}$$

If one qubit is encoded in N qubits, i.e., $d_R = 2$ and $d_A = 2^N$, we have, for $N \gg 1$,

$$\mathcal{F}_{\text{RE}}^{\text{Haar}} = 2^{-N+2}3[1 - g(\lambda)^{pN}]. \tag{A19}$$

[1] A. Nahum, S. Vijay, and J. Haah, Phys. Rev. X **8**, 021014 (2018).

[2] C. W. von Keyserlingk, T. Rakovszky, F. Pollmann, and S. L. Sondhi, Phys. Rev. X **8**, 021013 (2018).

[3] T. Zhou and A. Nahum, Phys. Rev. B **99**, 174205 (2019).

[4] V. Khemani, A. Vishwanath, and D. A. Huse, Phys. Rev. X **8**, 031057 (2018).

[5] T. Rakovszky, F. Pollmann, and C. W. von Keyserlingk, Phys. Rev. X **8**, 031058 (2018).

[6] P. Hayden, S. Nezami, X.-L. Qi, N. Thomas, M. Walter, and Z. Yang, J. High Energy Phys. 11 (2016) 009.

[7] F. Arute, K. Arya, R. Babbush, D. Bacon, J. C. Bardin, R. Barends, R. Biswas, S. Boixo, F. G. Brandao, D. A. Buell *et al.*, Nature (London) **574**, 505 (2019).

[8] A. Morvan, B. Villalonga, X. Mi, S. Mandrà, A. Bengtsson, P. Klimov, Z. Chen, S. Hong, C. Erickson, I. Drozdov *et al.*, arXiv:2304.11119.

[9] Y. Wu, W.-S. Bao, S. Cao, F. Chen, M.-C. Chen, X. Chen, T.-H. Chung, H. Deng, Y. Du, D. Fan *et al.*, Phys. Rev. Lett. **127**, 180501 (2021).

[10] Q. Zhu, S. Cao, F. Chen, M.-C. Chen, X. Chen, T.-H. Chung, H. Deng, Y. Du, D. Fan, M. Gong *et al.*, Sci. Bull. **67**, 240 (2022).

[11] W. Brown and O. Fawzi, in *2013 IEEE International Symposium on Information Theory, Istanbul, 2013* (IEEE, Piscataway, 2013), pp. 346–350.

[12] W. Brown and O. Fawzi, Commun. Math. Phys. **340**, 867 (2015).

[13] M. J. Gullans, S. Krastanov, D. A. Huse, L. Jiang, and S. T. Flammia, Phys. Rev. X **11**, 031066 (2021).

[14] S. Boixo, S. V. Isakov, V. N. Smelyanskiy, R. Babbush, N. Ding, Z. Jiang, M. J. Bremner, J. M. Martinis, and H. Neven, Nat. Phys. **14**, 595 (2018).

[15] D. Hangleiter and J. Eisert, Rev. Mod. Phys. **95**, 035001 (2023).

[16] A. M. Dalzell, N. Hunter-Jones, and F. G. S. L. Brandão, PRX Quantum **3**, 010333 (2022).

[17] F. G. S. L. Brandão, A. W. Harrow, and M. Horodecki, Commun. Math. Phys. **346**, 397 (2016).

[18] A. W. Harrow and S. Mehraban, Commun. Math. Phys. **401**, 1531 (2023).

[19] N. Hunter-Jones, arXiv:1905.12053.

[20] N. Lashkari, D. Stanford, M. Hastings, T. Osborne, and P. Hayden, J. High Energy Phys. 04 (2013) 022.

[21] E. Onorati, O. Buerschaper, M. Kliesch, W. Brown, A. H. Werner, and J. Eisert, Commun. Math. Phys. **355**, 905 (2017).

[22] G. S. Bentsen, S. Sahu, and B. Swingle, Phys. Rev. B **104**, 094304 (2021).

[23] S. Sahu, S.-K. Jian, G. Bentsen, and B. Swingle, Phys. Rev. B **106**, 224305 (2022).

[24] S.-K. Jian, G. Bentsen, and B. Swingle, J. High Energy Phys. 08 (2023) 190.

[25] G. Vidal, Phys. Rev. Lett. **91**, 147902 (2003).

[26] S. R. White and A. E. Feiguin, Phys. Rev. Lett. **93**, 076401 (2004).

[27] A. J. Daley, C. Kollath, U. Schollwöck, and G. Vidal, J. Stat. Mech. (2004) P04005.

[28] S.-K. Jian and B. Swingle, J. High Energy Phys. 11 (2023) 221.

[29] J. C. Napp, R. L. L. Placa, A. M. Dalzell, F. G. Brandão, and A. W. Harrow, Phys. Rev. X **12**, 021021 (2022).

[30] V. Balasubramanian, A. Kar, C. Li, O. Parrikar, and H. Rajgadia, J. High Energy Phys. 08 (2023) 071.

[31] B. Ware, A. Deshpande, D. Hangleiter, P. Niroula, B. Fefferman, A. V. Gorshkov, and M. J. Gullans, arXiv:2305.04954.

[32] A. M. Dalzell, N. Hunter-Jones, and F. G. S. L. Brandão, Commun. Math. Phys. **405**, 78 (2024).

[33] D. Aharonov, X. Gao, Z. Landau, Y. Liu, and U. Vazirani, in *Proceedings of the 55th Annual ACM Symposium on Theory of Computing, Orlando, 2023* (ACM, New York, 2023), pp. 945–957.

[34] B. Barak, C.-N. Chou, and X. Gao, Spoofing linear cross-entropy benchmarking in shallow quantum circuits, in *12th Innovations in Theoretical Computer Science Conference (ITCS 2021)*, Leibniz International Proceedings in Informatics (LIPIcs), Vol. 185 (Schloss Dagstuhl Leibniz-Zentrum für Informatik, 2021), pp. 30:1–30:20.

[35] X. Gao, M. Kalinowski, C.-N. Chou, M. D. Lukin, B. Barak, and S. Choi, PRX Quantum **5**, 010334 (2024).

[36] S.-K. Jian, C. Liu, X. Chen, B. Swingle, and P. Zhang, arXiv:2106.09635.

[37] B. Schumacher and M. A. Nielsen, Phys. Rev. A **54**, 2629 (1996).

[38] B. Schumacher and M. D. Westmoreland, arXiv:quant-ph/0112106.

[39] M.-D. Choi, Linear Algebra Appl. **10**, 285 (1975).

[40] A. Jamiołkowski, Rep. Math. Phys. **3**, 275 (1972).

[41] J. Hauschild and F. Pollmann, SciPost Phys. Lect. Notes **5**, 1 (2018); Code available from https://github.com/tenpy/tenpy.

[42] K. Binder and D. Landau, Phys. Rev. B **30**, 1477 (1984).

[43] F. G. S. L. Brandao and M. J. Kastoryano, arXiv:1609.07877.

[44] A. Abeyesinghe, I. Devetak, P. Hayden, and A. Winter, Proc. R. Soc. A **465**, 2537 (2009).

[45] C. Bény and O. Oreshkov, Phys. Rev. Lett. **104**, 120501 (2010).

[46] D. Abraham, Phys. Rev. Lett. **44**, 1165 (1980).

[47] Y. Li and M. P. A. Fisher, Phys. Rev. B **103**, 104306 (2021).

[48] Y. Li, S. Vijay, and M. P. A. Fisher, PRX Quantum **4**, 010331 (2023).

[49] I. Lovas, U. Agrawal, and S. Vijay, arXiv:2304.02664.

[50] Z. Li, S. Sang, and T. H. Hsieh, Phys. Rev. B **107**, 014307 (2023).

[51] S.-K. Jian, C. Liu, X. Chen, B. Swingle, and P. Zhang, Phys. Rev. Lett. **127**, 140601 (2021).